
Physics-Integrated Variational Autoencoders for Robust and Interpretable Generative Modeling

Naoya Takeishi, Alexandros Kalousis

University of Applied Sciences and Arts Western Switzerland (HES-SO)
Geneva, Switzerland

{naoya.takeishi,alexandros.kalousis}@hesge.ch

Abstract

Integrating physics models within machine learning models holds considerable promise toward learning robust models with improved interpretability and abilities to extrapolate. In this work, we focus on the integration of incomplete physics models into deep generative models. In particular, we introduce an architecture of variational autoencoders (VAEs) in which a part of the latent space is grounded by physics. A key technical challenge is to strike a balance between the incomplete physics and trainable components such as neural networks for ensuring that the physics part is used in a meaningful manner. To this end, we propose a regularized learning method that controls the effect of the trainable components and preserves the semantics of the physics-based latent variables as intended. We not only demonstrate generative performance improvements over a set of synthetic and real-world datasets, but we also show that we learn robust models that can consistently extrapolate beyond the training distribution in a meaningful manner. Moreover, we show that we can control the generative process in an interpretable manner.

1 Introduction

Data-driven modeling is often opposed to theory-driven modeling, yet their integration has also been recognized as an important approach called *gray-box* or *hybrid* modeling. In statistical machine learning, incorporation of mathematical models of physics (in a broad sense; including knowledge of biology, chemistry, economics, etc.) has also been attracting attention. Gray-box / hybrid modeling in machine learning holds considerable promise toward learning robust models with improved abilities to extrapolate beyond the distributions that they have been exposed to during training. Moreover, it can bring significant benefits in terms of model interpretability since parts of a model get semantically grounded to concrete domain knowledge.

A technical challenge in *deep* gray-box modeling is to ensure an appropriate use of physics models. A careless design of models and learning can lead to an erratic behavior of the components meant to represent physics (e.g., with erroneous estimation of physics parameters), and eventually, the overall model just learns to ignore them. This is particularly the case when we bring together simplified or imperfect physics models with highly expressive data-driven machine learning models such as deep neural networks. Such cases call for principled methods for striking an appropriate balance between physics and data-driven models to prevent the detrimental effects during learning.

Integration of physics models into machine learning has been considered in various contexts (see, e.g., [99, 94] and our Section 4), but most existing studies focus on prediction or forecasting tasks and are not directly applicable to other tasks. More importantly, the careful orchestration of physics-based and data-driven components have not necessarily been considered. A notable exception is Yin et al. [104], in which they proposed a method to regularize the action of trainable components of a hybrid

model of differential equations. Their method has been developed for dynamics forecasting with additive combinations of physics and trainable models, but application to other situations is not trivial.

In this work, we aim at the integration of incomplete physics models into deep generative models. While we focus on variational autoencoders (VAEs, [43, 75]), our idea is applicable to other models in principle. In our VAE, the decoder comprises physics-based models and trainable neural networks, and some of the latent variables are semantically grounded to the parameters of the physics models. Such a VAE, if appropriately trained, is by construction partly interpretable. Moreover, since it can by construction capture the underlying physics, it will be robust in out-of-distribution regime and exhibit meaningful extrapolation properties. We propose a regularized learning framework for ensuring the meaningful use of the physics models and the preservation of the semantics of the latent variables in the physics-integrated VAEs. We empirically demonstrate that our method can learn a model that exhibits better generalization, and more importantly, can extrapolate robustly in out-of-distribution regime. In addition, we show how the direct access to the physics-grounded latent variables allows us to alter properties of generation meaningfully and explore counterfactual scenarios.

2 Physics-integrated VAEs

We first describe the structure of VAEs we consider, which comprise physics models and machine learning models such as neural nets. We suppose that the physics models can be solved analytically or numerically with a reasonable cost, and the (approximate) solution is differentiable with regard to the quantities on which the solution depends. This assumption holds in most physics models known in practice, which come in different forms such as algebraic and differential equations. If there is no closed-form solution of algebraic equations, we can utilize differentiable optimizers [4] as a layer of the model. For differential equations, differentiable integrators [see, e.g., 14] will constitute a layer. Handling non-differentiable and/or overly-complex simulators remains an important open challenge.

2.1 Example

We start with an example to demonstrate the main concepts. Let us suppose that data comprise time-series of the angle of pendulums following an ordinary differential equation (ODE):

$$\underbrace{d^2\vartheta(t)/dt^2 + \omega^2 \sin \vartheta(t)}_{\text{given as prior knowledge, } f_P} + \underbrace{\xi d\vartheta(t)/dt - u(t)}_{\text{to be learned by NN, } f_A} = 0, \quad (1)$$

where ϑ is a pendulum’s angle, and ω , ξ , and u are the pendulum’s angular velocity, damping coefficient, and external force, respectively. We suppose that a data point x is a sequence of $\vartheta(t)$, i.e., $x = [\vartheta(0) \ \vartheta(\Delta t) \ \cdots \ \vartheta((\tau - 1)\Delta t)]^T \in \mathbb{R}^\tau$ for some $\Delta t \in \mathbb{R}$ and $\tau \in \mathbb{N}$, where $\vartheta(t)$ denotes the solution of (1) with a particular configuration of ω , ξ , and u . In this example, we learn a VAE on a dataset comprising such x ’s with different configurations of ω , ξ , and u .

Suppose that the first two terms of (1) are given as prior knowledge, i.e., we know that the governing equation should contain $f_P(\vartheta, z_P) := \ddot{\vartheta} + z_P^2 \sin \vartheta$. We will use such prior knowledge, f_P , by incorporating it in the decoder of a VAE that we will learn. Since f_P misses some effects of the true system (1), we complete it by augmenting the decoder with a neural network $f_A(\vartheta, z_A)$. The VAE’s latent variable will have two parts, z_P and z_A , respectively linked to f_P and f_A . On one hand, z_A works as an ordinary VAE’s latent variable since f_A is a neural net, and we suppose $z_A \in \mathbb{R}^d$, $p(z_A) := \mathcal{N}(\mathbf{0}, \mathbf{I})$. On the other hand, we semantically ground z_P to a physics parameter; in this case, $z_P \in \mathbb{R}$ should work as pendulum’s ω . In summary, the augmented decoder here is $\mathbb{E}[x] = \text{ODEsolve}_\vartheta [f_P(\vartheta(t), z_P) + f_A(\vartheta(t), z_A) = 0]$, where $\text{ODEsolve}_\vartheta$ denotes some differentiable solver of an ODE with regard to ϑ . The encoder will have corresponding recognition networks for z_P and z_A . The situation in this example will be numerically examined in Section 5.1.

2.2 General formulation

We now present the concept of our physics-integrated VAEs in a general form. Note that our interest is not limited to the additive model combination nor ODEs. In fact, the general formulation below subsumes non-additive augmentation of various physics models. The notation introduced in this section will be used to explain the proposed regularized learning method later in Section 3.

For ease of discussion, we suppose that a VAE decoder comprises two parts: a physics-based model f_P and a trainable auxiliary function f_A . More general cases, for example with multiple trainable functions $f_{A,1}, f_{A,2}, \dots$ used in different ways, are handled in Appendix A.

2.2.1 Latent variables and priors

We consider two types of latent variables, $z_P \in \mathcal{Z}_P$ and $z_A \in \mathcal{Z}_A$, which respectively will be used in f_P and f_A . The latent variables can be in any space, but for the sake of discussion, we suppose \mathcal{Z}_P and \mathcal{Z}_A are (subsets of) the Euclidean space and set their prior distribution as multivariate normal:

$$p(z_P) := \mathcal{N}(z_P \mid \mathbf{m}_P, v_P^2 \mathbf{I}) \quad \text{and} \quad p(z_A) := \mathcal{N}(z_A \mid \mathbf{0}, \mathbf{I}), \quad (2)$$

where \mathbf{m}_P and v_P^2 are defined in accordance with prior knowledge of f_P 's parameters. Note that z_P will be directly interpretable as they will be semantically grounded to the parameters of the physics model f_P ; for example in Section 2.1, $z_P := \omega$ was the angular velocity of a pendulum.

2.2.2 Decoder

The decoder of a physics-integrated VAE comprises two types of functions¹, $f_P: \mathcal{Z}_P \rightarrow \mathcal{Y}_P$ and $f_A: \mathcal{Y}_P \times \mathcal{Z}_A \rightarrow \mathcal{Y}_A$. For notational convenience, we consider a functional \mathcal{F} that evaluates f_P and f_A , solves an equation if any, and finally gives observation $\mathbf{x} \in \mathcal{X}$. \mathcal{X} may be the space of sequences, images, and so on. Assuming Gaussian observation noise, we write the observation model as

$$p_\theta(\mathbf{x} \mid z_P, z_A) := \mathcal{N}(\mathbf{x} \mid \mathcal{F}[f_A, f_P; z_P, z_A], \Sigma_x), \quad (3)$$

where $z_A \in \mathcal{Z}_A$ and $z_P \in \mathcal{Z}_P$ are the arguments of f_A and f_P , respectively. Note that f_A and f_P may have other arguments besides z_A and z_P , respectively, but they are omitted for simplicity. We denote the set of trainable parameters of f_A and f_P (and Σ_x) by θ , while f_P may have no trainable global parameters other than z_P .

Let us see the semantics of the functional² \mathcal{F} first in the light of the example of Section 2.1. Recall that there we considered the additive augmentation of ODE (as in [104] and other studies). It is subsumed by the expression (3) by setting $\mathcal{F}[f_A, f_P; z_P, z_A] := \text{ODEsolve}[f_P(z_P) + f_A(z_A) = 0]$. Let us generalize the idea. Our definition of the decoder in (3) allows not only additive augmentation of ODE but also broader range of architectures. The composition of f_P and f_A is not limited to be additive because we consider general composition of functions f_A and f_P . Moreover, the form of the physics model is not limited to ODEs. We list some examples of the configuration:

- If equation $f_P = 0$ has a closed-form solution $S_{f_P} \in \mathcal{Y}_P$ (assuming that the solution space coincides with \mathcal{Y}_P , just for ease of discussion), then \mathcal{F} is simply an evaluation of f_A , for example, $\mathcal{F}[f_P, f_A; z_A] := f_A(S_{f_P}, z_A)$.
- If an algebraic equation $f_P = 0$ or $f_A \circ f_P = 0$ has no closed-form solution, then \mathcal{F} will have a differentiable optimizer, e.g., $\mathcal{F}[f_P, f_A] := f_A(\arg \min \|f_P\|^2)$ or $\mathcal{F} := \arg \min \|f_A \circ f_P\|^2$.
- $f_P = 0$ or $f_A \circ f_P = 0$ can be a stochastic differential equation (and \mathcal{F} contains its solver), for which z_P and/or z_A would become a sequence encoding the realization of the process noise.

The role of f_A can also be diverse; it can work not only as a complement of physics models inside equations, but also as correction of numerical errors of solvers or optimizers, downsampling or upsampling, and observables (e.g., from angle sequence to video of a pendulum).

2.2.3 Encoder

The encoder of a physics-integrated VAE accordingly comprises two parts: for posterior inference of z_P and for that of z_A . We consider the following decomposition of the approximated posterior:

$$q_\psi(z_P, z_A \mid \mathbf{x}) := q_\psi(z_A \mid \mathbf{x})q_\psi(z_P \mid \mathbf{x}, z_A), \quad (4)$$

where $q_\psi(z_A \mid \mathbf{x}) := \mathcal{N}(z_A \mid g_A(\mathbf{x}), \Sigma_A)$, $q_\psi(z_P \mid \mathbf{x}, z_A) := \mathcal{N}(z_P \mid g_P(\mathbf{x}, z_A), \Sigma_P)$.

¹The distinction between f_P and f_A depends on the origin of the functional forms (and not if trainable or not). The form of f_P depends on physics' insight and thus fixed. On the other hand, the form of f_A is determined only from utility as a function approximator, and we can use whatever useful (e.g., feed-forward NNs, RNNs, etc.).

²It is natural to consider that \mathcal{F} is a functional (and not a function) because we may need the access to the functions f_A and f_P themselves, rather than their pointwise values. For example, we need the full access to those functions when the decoder has an ODE solver with arbitrary initial condition.

$g_A: \mathcal{X} \rightarrow \mathcal{Z}_A$ and $g_P: \mathcal{X} \times \mathcal{Z}_A \rightarrow \mathcal{Z}_P$ are recognition networks. We denote the trainable parameters of g_A and g_P (and Σ_A and Σ_P) as ψ . This particular dependency is for our regularization method in Section 3.2, where g_P should first remove the information of z_A from \mathbf{x} and then infer z_P .

2.3 Evidence lower bound

The VAE is to be learned as usual by maximizing the lower bound of the marginal log likelihood known as evidence lower bound (ELBO). In our case, it is straightforward to derive:

$$\begin{aligned} \text{ELBO}(\theta, \psi; \mathbf{x}) = & \mathbb{E}_{q_\psi(z_P, z_A | \mathbf{x})} \log p_\theta(\mathbf{x} | z_P, z_A) \\ & - D_{\text{KL}}[q_\psi(z_A | \mathbf{x}) \| p(z_A)] - \mathbb{E}_{q_\psi(z_A | \mathbf{x})} D_{\text{KL}}[q_\psi(z_P | \mathbf{x}, z_A) \| p(z_P)]. \end{aligned} \quad (5)$$

3 Striking balance between physics and trainable models

We propose a regularized learning objective for physics-integrated VAEs. It comprises two types of regularizers. The first is for regularizing unnecessary flexibility of function approximators like neural networks and presented in Section 3.1. The second is for grounding encoder’s output to physics parameters and presented in Section 3.2. The overall objective is summarized in Section 3.3.

3.1 Regularizing excess flexibility of trainable functions

If the trainable component of the physics-integrated VAE (i.e., f_A) has rich expression capability, as is often the case with deep neural networks, merely maximizing the ELBO in (5) provides no guarantee that the physics-based component (i.e., f_P) will be used in a meaningful manner; e.g., f_P may just be ignored. We want to ensure that f_A does not unnecessarily dominate the behavior of the entire model and that f_P is not ignored. To this end, we borrow an idea from the *posterior predictive check* (PPC), a procedure to check the validity of a statistical model [see, e.g., 26]. Whereas the standard PPCs examine the discrepancy between distributions of a model and data, we compute the discrepancy between those of the model and its “physics-only” reduced version, for monitoring and balancing the contributions of parts of the model.

For the sake of argument, suppose that a given physics model f_P is completely correct for given data. Then, the discrepancy between the original model and its “physics-only” reduced model (where f_A is somehow invalidated) should be close to zero because the decoder of both the original model (with f_P and f_A working) and the reduced model (with only f_P working) should coincide in an ideal limit with the true data-generating process. Even if f_P captures only a part of the truth, the discrepancy should be kept small, if not zero, to ensure meaningful use of the physics models in the overall model.

The “physics-only” reduced model is created as follows. Recall that the original VAE is defined by Eqs. (3) and (4). We define the decoder of the reduced model by replacing $f_A: \mathcal{Y}_P \times \mathcal{Z}_A \rightarrow \mathcal{Y}_A$ of (3) with a *baseline function* $h_A: \mathcal{Y}_P \rightarrow \mathcal{Y}_A$. That is, the reduced observation model is

$$p_{\theta^r}^r(\mathbf{x} | z_P, z_A) := \mathcal{N}(\mathbf{x} | \mathcal{F}[h_A, f_P; z_P], \Sigma_x), \quad (3r)$$

where we omit z_A from the argument of \mathcal{F} because h_A no longer takes it. We denote the set of the trainable parameters of such a model as $\theta^r := \theta \setminus \text{param}(f_A) \cup \text{param}(h_A)$. The corresponding encoder is defined as follows. Recall that in the original model, posterior distributions of both z_P and z_A are inferred in (4) and then used for reconstructing each input \mathbf{x} in (3). On the other hand, in the “physics-only” reduced model, z_A is not referred to by (3r), which makes it less meaningful to place a particular posterior of z_A for each \mathbf{x} . Hence, we define the “physics-only” encoder by marginalizing out z_A and using prior³ $p(z_A)$ instead. That is, the reduced posterior is

$$q_\psi^r(z_A, z_P | \mathbf{x}) := p(z_A) \int q_\psi(z_P, z_A | \mathbf{x}) dz_A. \quad (4r)$$

Below we give a guideline for the choice of the baseline function, h_A :

- If the ranges of f_P and f_A are the same (i.e., $\mathcal{Y}_P = \mathcal{Y}_A$), then h_A can be an identity function $h_A = \text{Id}$. Note that in the additive case $f_A \circ f_P = f_P + f_{A'}$, where $f_{A'}$ is a trainable function, replacing f_A with $h_A = \text{Id}$ is equivalent to replacing $f_{A'}$ with $h_{A'} = 0$.

³It is just for defining q_ψ^r on the common support with q_ψ . Any non-informative distributions of z_A are fine.

- If $\mathcal{Y}_P \neq \mathcal{Y}_A$, then h_A can be a linear or affine map from \mathcal{Y}_P to \mathcal{Y}_A . For example, if $\mathcal{Y}_P = \mathbb{R}^{d_P}$ and $\mathcal{Y}_A = \mathbb{R}^{d_A}$ ($d_P \neq d_A$), then we can set $h_A(f_P(z_P)) = \mathbf{W} f_P(z_P)$ where $\mathbf{W} \in \mathbb{R}^{d_A \times d_P}$.

The idea is to minimize the discrepancy between the full model and the ‘‘physics-only’’ reduced model. In particular, we minimize the discrepancy between the posterior predictive distributions

$$D_{\text{KL}}[p_{\theta, \psi}(\tilde{\mathbf{x}} | X) \| p_{\theta^r, \psi}^r(\tilde{\mathbf{x}} | X)], \quad \text{where}$$

$$p_{\theta, \psi}(\tilde{\mathbf{x}} | X) = \int p_{\theta}(\tilde{\mathbf{x}} | z_P, z_A) q_{\psi}(z_P, z_A | \mathbf{x}) p_d(\mathbf{x} | X) dz_P dz_A d\mathbf{x}, \quad (6)$$

$$p_{\theta^r, \psi}^r(\tilde{\mathbf{x}} | X) = \int p_{\theta^r}^r(\tilde{\mathbf{x}} | z_P, z_A) q_{\psi}^r(z_P, z_A | \mathbf{x}) p_d(\mathbf{x} | X) dz_P dz_A d\mathbf{x}.$$

$p_d(\mathbf{x} | X)$ is the empirical distribution with the support on data $X := \{\mathbf{x}_1, \dots, \mathbf{x}_n\}$. We use $\tilde{\mathbf{x}}$, instead of \mathbf{x} , just for avoiding notational confusion by clarifying the target of integral $\int d\mathbf{x}$.

Unfortunately, analytically computing (6) is usually intractable. Hence, we take the following upper bound of (6) (a proof is in Appendix B, and further remarks are in Appendix C):

Proposition 1. *Let p_{θ} and p_{θ}^r be the shorthand of $p_{\theta}(\tilde{\mathbf{x}} | z_P, z_A)$ in (3) and $p_{\theta^r}^r(\tilde{\mathbf{x}} | z_P, z_A)$ in (3r), respectively. Let p_P and p_A be some distributions of z_P and z_A , e.g., $p(z_P)$ and $p(z_A)$ using the priors in (2), respectively. The KL divergence in (6) can be upper bounded as follows:*

$$D_{\text{KL}}[p_{\theta, \psi}(\tilde{\mathbf{x}} | X) \| p_{\theta^r, \psi}^r(\tilde{\mathbf{x}} | X)] \leq \mathbb{E}_{p_d(\mathbf{x}|X)} \left[\mathbb{E}_{q_{\psi}(z_P, z_A | \mathbf{x})} D_{\text{KL}}[p_{\theta} \| p_{\theta}^r] \right. \\ \left. + D_{\text{KL}}[q_{\psi}(z_A | \mathbf{x}) \| p_A] + \mathbb{E}_{q_{\psi}(z_A | \mathbf{x})} D_{\text{KL}}[q_{\psi}(z_P | z_A, \mathbf{x}) \| p_P] \right]. \quad (7)$$

Definition 1. Let us denote the upper bound (7) by $\mathbb{E}_{p_d(\mathbf{x}|X)} \hat{D}(\theta, \text{param}(h), \psi; \mathbf{x})$. The regularization for inhibiting unnecessary flexibility of trainable functions is defined as minimization of

$$R_{\text{PPC}}(\theta, \text{param}(h), \psi) := \mathbb{E}_{p_d(\mathbf{x}|X)} \hat{D}(\theta, \text{param}(h), \psi; \mathbf{x}). \quad (8)$$

Remark 1. When multiple trainable functions are differently used in a model (e.g., inside and outside an equation solver), which is often the case in practice, the definition of R_{PPC} should be generalized to consider marginal contribution of every trainable function. See Appendix A.

3.2 Grounding physics encoder by physics-based data augmentation

Toward properly learning physics-integrated VAEs, minimizing R_{PPC} solely may not be enough because inferred z_P may be still meaningless but makes R_{PPC} not that large (e.g., with solution of f_P fluctuating around the mean pattern of data), and then optimization may not be able to escape such local minima. Though it is difficult to avoid such a local solution perfectly, we can alleviate the situation by considering additional objectives to encourage a proper use of the physics.

The idea is to use the physics model as a source of information for data augmentation, which helps us to ground the output of the recognition network, g_P in (4), to the parameters of f_P . We want to draw some z_P , feed it to the physics model f_P (and a solver if any), and use the generated signal as additional data during training. A technical challenge to this end is that because the physics model may be incomplete, the artificial signals from it and the real signals may have different natures. To compensate such difference, we arrange a particular functionality of the physics encoder, g_P .

Let z_P^* be a sample drawn from some distribution of z_P (e.g., prior $p(z_P)$). We artificially generate signals $\mathbf{x}^r(z_P^*)$ by feeding z_P^* to the ‘‘physics-only’’ decoding process in (3r), that is,

$$\mathbf{x}^r(z_P^*) := \mathcal{F}[h_A, f_P; z_P = z_P^*]. \quad (9)$$

We want the physics-part recognition network, g_P , to successfully estimate z_P^* given the corresponding $\mathbf{x}^r(z_P^*)$, which is necessary to say that the result of the inference by g_P is grounded to the parameters of f_P . However, in general, real data \mathbf{x} and the augmented data $\mathbf{x}^r(z_P^*)$ have different natures because f_P may miss some aspects of the true data-generating process.

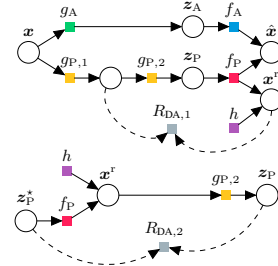


Figure 1: Diagrams of (upper) $R_{\text{DA},1}$ in (11) and (lower) $R_{\text{DA},2}$ in (12).

We handle this issue by considering a specific design of the physics-part recognition network, g_P . We decompose g_P into two stages as $g_P(\mathbf{x}, \mathbf{z}_A) = g_{P,2}(g_{P,1}(\mathbf{x}, \mathbf{z}_A))$ without loss of generality. On one hand, $g_{P,1}$ should transform real data \mathbf{x} to signals that resemble the physics-based augmented signal, \mathbf{x}^r . In other words, $g_{P,1}$ should “cleansed” real data into a virtual “physics-only” counterpart. We enforce such a functionality of $g_{P,1}$ by making its output close to the following quantity:

$$\mathbf{x}^r(g_P(\mathbf{x}, \mathbf{z}_A)) = \mathcal{F}[h_A, f_P; \mathbf{z}_P = g_P(\mathbf{x}, \mathbf{z}_A)]. \quad (10)$$

On the other hand, $g_{P,2}$ should receive such “cleansed” input and return the (sufficient statistics of) posterior of \mathbf{z}_P . If the aforementioned functionality of $g_{P,1}$ is successfully realized, we can directly self-supervise $g_{P,2}$ with $\mathbf{x}^r(\mathbf{z}_P^*)$ because $\mathbf{x}^r(g_P(\mathbf{x}, \mathbf{z}_A))$ and $\mathbf{x}^r(\mathbf{z}_P^*)$ should have similar nature.

In summary, we define a couple of regularizers for setting such functionality of $g_{P,1}$ and $g_{P,2}$ as follows (with the corresponding diagrams of computation shown in Figure 1):

Definition 2. Let $\text{sg}[\cdot]$ be the stop-gradient operator. The regularization for the physics-based data augmentation is defined as minimization of

$$R_{\text{DA},1}(\psi) := \mathbb{E}_{p_d(\mathbf{x}|X)q(\mathbf{z}_A|\mathbf{x})} \|g_{P,1}(\mathbf{x}, \mathbf{z}_A) - \text{sg}[\mathbf{x}^r(g_P(\mathbf{x}, \mathbf{z}_A))]\|_2^2 \quad \text{and} \quad (11)$$

$$R_{\text{DA},2}(\psi) := \mathbb{E}_{z_P^*} \|g_{P,2}(\text{sg}[\mathbf{x}^r(\mathbf{z}_P^*)]) - z_P^*\|_2^2. \quad (12)$$

3.3 Overall regularized learning objective

The overall regularized learning problem of the proposed physics-integrated VAEs is as follows:

$$\underset{\theta, \text{param}(h), \psi}{\text{minimize}} \quad -\mathbb{E}_{p_d(\mathbf{x}|X)} \text{ELBO}(\theta, \psi; \mathbf{x}) + \alpha R_{\text{PPC}}(\theta, \text{param}(h), \psi) + \beta R_{\text{DA},1}(\psi) + \gamma R_{\text{DA},2}(\psi),$$

where each term appears in (5), (8), (11), and (12), respectively. Recall that θ and ψ are the sets of the parameters of the full model’s decoder (3) and encoder (4), respectively, and that $\text{param}(h)$ denotes the set of the parameters of h , which may be empty. If we cannot specify a reasonable sampling distribution of \mathbf{z}_P^* needed in (12), we do not use $R_{\text{DA},1}$ and $R_{\text{DA},2}$; it may happen when the semantics of \mathbf{z}_P are not inherently grounded, e.g., when f_P is a *neural* Hamilton’s equation [91].

4 Related work

The integration of theory-driven and data-driven methodologies has been sought in various ways. We overview some perspectives in this section and more in Appendix D.

Physics+ML in model design Integration in model design, often called gray-box or hybrid modeling, has been studied for decades [e.g., 67, 76, 90] and is still active, with deep neural networks utilized in various areas [e.g., 105, 70, 53, 96, 63, 1, 2, 19, 106, 97, 79, 46, 61, 10, 82, 69, 50, 68, 84]. Most recent studies focus on prediction, and the generative modeling has been less investigated. Moreover, mechanisms to regularize the flexibility of trainable components have hardly been addressed.

The work of Yin et al. [104] is notable here because they consider a mechanism to regularize the flexibility a trainable component to preserve the utility of physics in the model, even though it is only focused on dynamics learning for forecasting. They learn an additive hybrid ODE model $\dot{x} = f_P(x) + f_A(x)$, where f_P is a prescribed physics model, and f_A is a neural network. Such a model is subsumed in our architecture as exemplified in Section 2. Moreover, Yin et al. [104] propose to regularize f_A by minimizing $\|f_A\|_2^2$. Such a term also appears in one of our regularizers, R_{PPC} ; when the observation noise is Gaussian, the first term of the right-hand side of (7) becomes $\mathbb{E}\|(f_A \circ f_P) - f_P\|_2^2 = \mathbb{E}\|f_P + f_A - f_P\|_2^2 = \mathbb{E}\|f_A\|_2^2$. Therefore, we get a “VAE variant” of Yin et al. [104] by switching off a part of R_{PPC} and the other regularizers, $R_{\text{DA},1}$ and $R_{\text{DA},2}$. We examine cases similar to it in our experiment for comparison.

Yıldız et al. [103] and Linial et al. [52] developed VAEs whose latent variable follows ODEs. Linial et al. [52] also suggest grounding the semantics of the latent variable by providing sparse supervision on it. It is feasible only when we have a chance to observe the latent variable (e.g., with an increased cost) and may often be inherently infeasible in some problem settings including ours. In our method, we never assume availability of observation of latent variables and instead use the physics models in a self-supervised manner. While direct comparison is not meaningful due to the difference of settings, we examine a baseline close to the base model of Linial et al. [52] in our experiment for comparison.

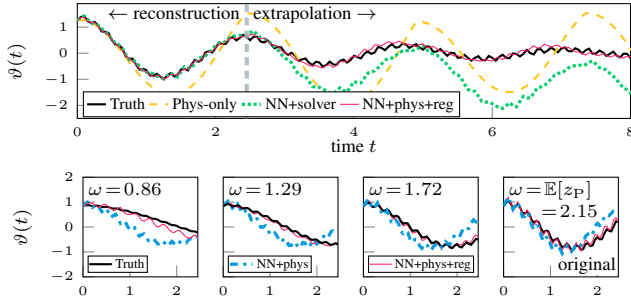


Figure 2: Reconstruction and extrapolation of a test sample of the pendulum data. Range $0 \leq t < 2.5$ is reconstruction, whereas $t \geq 2.5$ is extrapolation.

Figure 3: Counterfactual generation for the pendulum data. Horizontal axis is time t . The center panel shows the original data, and the rest is the generation with z_P (i.e., ω) altered while z_A fixed.

Toth et al. [91] propose a model where the latent variable sequence is governed by the Hamiltonian mechanics with a neural Hamiltonian. While it does not suppose very specific physics models but considers general mechanics, they can also be included in our framework; that is, f_P can be a Hamilton’s equation with a neural Hamiltonian. We try such a model in one of our experiments.

Physics+ML in objective design Another prevailing strategy is to define objective functions based on physics knowledge [e.g., 86, 41, 71, 33, 102, 36, 107, 77, 13, 98]. In generative modeling, for example, Stinis et al. [87] use residuals from physics models as a feature of GAN’s discriminator. Golany et al. [27] regularize the generation from GANs by forcing it close to a prescribed physics relation. These approaches are often easy to deploy, but an inherent limitation is that given physics knowledge should be complete to some extent, otherwise a physics-based loss is not well-defined.

5 Experiments

We performed experiments on two synthetic datasets and two real-world datasets, for which we prepared instances of physics-integrated VAEs. We show each particular architecture of physics-integrated VAEs and the corresponding results; some details are deferred to Appendix E. While direct comparison is impossible due to the differences of the problem settings, the baseline methods we examined (listed below) are similar to some existing methods [5, 103, 91, 52, 104].

NN-only	Ordinary VAE [43, 75]; the decoder is $\mathbb{E}x = f_A(z_A)$, where f_A is a neural net.
Phys-only	Physics VAE; the decoder is $\mathbb{E}x = \mathcal{F}[f_P; z_P]$ with no neural nets. The encoder is with neural nets as ordinary VAEs. This is almost equivalent to the method of Aragon-Calvo and Carvajal [5] when the problem is as in Section 5.3.
NN+solver	VAE with physics solvers; the decoder is $\mathbb{E}x = \mathcal{F}[f_A; z_A]$, where f_A is a neural net, and \mathcal{F} includes some equation-solving process (e.g., ODE/PDE solver), but no more physics-based knowledge is given (i.e., there is no f_P). This is similar to the methods of, for example, Yıldız et al. [103] and Toth et al. [91].
NN+phys	Physics-integrated VAE learned without the regularizers (i.e., $\alpha = \beta = \gamma = 0$); this is similar to the base models of Linial et al. [52] and Qian et al. [68]. Finer ablations are also studied, among which the cases with $\beta = 0$ or $\gamma = 0$ are similar to the model of Yin et al. [104].
NN+phys+reg	Our proposal; physics-integrated VAE learned with the proposed regularizers.

We aligned the total dimensionality of the latent variables of each method (except phys-only); when $\dim z_A = d_A$ and $\dim z_P = d_P$ in NN+phys(+reg), we set $\dim z_A = d_A + d_P$ in NN-only and NN+solver. The hyperparameters, α , β , and γ , were chosen with validation set performance. We investigated the performance sensitivity to them; no large degradation of performance was observed even if we changed the values by $\times 10$ or $\times \frac{1}{10}$ from the chosen values; details are in Appendix F.

5.1 Forced damped pendulum

Dataset We generated data from (1) with $u(t) = A\omega^2 \cos(2\pi\phi t)$. Each data-point x is a sequence $x := [\vartheta_1 \cdots \vartheta_r] \in \mathbb{R}^r$, where ϑ_j is the value of a solution $\vartheta(t_j)$ at $t_j := (j-1)\Delta t$. We randomly

Table 1: Reconstruction errors and inference errors on test sets of the pendulum data and the advection-diffusion data. Averages (and SDs) over 20 random trials are reported.

		Pendulum				Advection-diffusion			
		MAE of reconstr.		MAE of inferred ω		MAE of reconstr.		MAE of inferred a	
NN-only		0.438	(2.9×10^{-2})	–	–	0.0396	(2.2×10^{-4})	–	–
Phys-only		1.55	(7.1×10^{-4})	0.232	(5.9×10^{-3})	0.393	(9.5×10^{-4})	0.0103	(1.5×10^{-3})
NN+solver		0.439	(2.3×10^{-2})	–	–	0.0388	(1.7×10^{-4})	–	–
NN+phys		0.370	(4.3×10^{-2})	1.04	(2.2×10^{-1})	0.0404	(1.2×10^{-2})	0.258	(3.2×10^{-1})
NN+phys+reg		0.363	(4.8×10^{-2})	0.229	(3.8×10^{-2})	0.0437	(1.5×10^{-3})	0.00951	(6.2×10^{-3})
Ablations	$\alpha = 0$	0.396	(4.3×10^{-2})	0.889	(1.9×10^{-1})	0.0461	(1.3×10^{-2})	0.0444	(1.4×10^{-2})
	$\beta = 0$	0.372	(4.1×10^{-2})	0.223	(3.6×10^{-2})	0.0747	(2.4×10^{-2})	0.199	(2.3×10^{-1})
	$\gamma = 0$	0.381	(4.1×10^{-2})	0.276	(4.2×10^{-2})	0.0588	(9.1×10^{-4})	0.0548	(9.4×10^{-7})

drew a sample of the initial condition ϑ_1 (with $\dot{\vartheta}_1 = 0$ fixed) and the values of ω , ζ , A , and ϕ for each sequence. We generated 2,500 sequences of length $\tau = 50$ with $\Delta t = 0.05$ and separated them into a training, validation, and test sets with 1,000, 500, and 1,000 sequences, respectively.

Setting We set f_P as in Section 2.1, i.e., $f_P(\vartheta, z_P) := \ddot{\vartheta} + z_P^2 \sin(\vartheta)$, where $z_P \in \mathbb{R}$ should work as angular velocity ω . We augmented it by $f_{A,1}(\vartheta, z_{A,1})$ additively, where $f_{A,1}$ was a multi-layer perceptron (MLP) and $z_{A,1} \in \mathbb{R}$. The ODE $f_P + f_{A,1} = 0$ was solved with the Euler update scheme in the model. The model had another MLP⁴ $f_{A,2}$ with another latent variable $z_{A,2} \in \mathbb{R}^2$ for further modifying the solution of the ODE. In summary, the decoding process is $\mathcal{F} := f_{A,2}(\text{solve}_{\vartheta}[f_P(\vartheta, z_P) + f_{A,1}(\vartheta, z_{A,1}) = 0], z_{A,2})$. The construction of the proposed regularizer for such multiple f_A 's is elaborated in Appendix A. We used $h_{A,1} = 0$ and $h_{A,2} = \text{Id}$ as the baseline functions. The recognition networks, $g_{A,1}$, $g_{A,2}$, and g_P , were modeled with MLPs. We used the initial element of each \mathbf{x} as an estimation of the initial condition ϑ_1 .

Results Figure 2 demonstrates a unique benefit of the hybrid modeling. We show an example of reconstruction with extrapolation. Recall that the training data comprise sequences of range $0 \leq t < 2.5$ only; so the results in $t \geq 2.5$ are extrapolation (in time) rather than mere reconstruction. We can observe that while NN+solver cannot extrapolate even if it is equipped with a neural ODE, NN+phys+reg can reconstruct and extrapolate correctly.

Figure 3 illustrates well the advantage of the proposed regularizers. We show an example of generation from learned models with z_P manipulated. Recall that z_P is expected to work as pendulum's angular velocity ω . We took a test sample with $\omega \approx \mathbb{E}[z_P] \approx 2.15$ and generated signals with the original and different values of z_P , keeping the values of z_A to be the original posterior mean. We can see that the generation from NN+phys+reg matches better with the signals from the true process.

Table 1 (left half) summarizes the performance in terms of the reconstruction error and the inference error of physics parameter ω on the test set. The errors are reported in mean absolute errors (MAEs). The inference error of ω is evaluated by $|\mathbb{E}[z_P] - \omega_{\text{true}}|$. NN+phys+reg achieves small values in *both* reconstruction error and inference error. Meanwhile, the MAE of reconstruction by phys-only is significantly worse than those of the other methods, and the MAE of ω inferred by NN+phys is significantly worse than the others. These facts imply the effectiveness of the hybrid modeling and the proposed regularizers.

5.2 Advection-diffusion system

Dataset We generated data from advection-diffusion PDE $\partial T / \partial t - a \cdot \partial^2 T / \partial s^2 + b \cdot \partial T / \partial s = 0$, where s is the 1-D spatial dimension. We approximated the solution $T(s, t)$ on the 12-point even grid from $s = 0$ to $s = s_{\text{max}}$, so each data-point \mathbf{x} is a sequence of 12-dim vectors, i.e., $\mathbf{x} := [\mathbf{T}_1 \cdots \mathbf{T}_\tau] \in \mathbb{R}^{12 \times \tau}$, where $\mathbf{T}_j := [T(0, t_j) \cdots T(s_{\text{max}}, t_j)]^\top$ at $t_j := (j - 1)\Delta t$. We set the boundary condition as $T(0, t) = T(s_{\text{max}}, t) = 0$ and the initial condition as $T(s, 0) = c \sin(\pi s / s_{\text{max}})$. We randomly drew a , b , and c for each \mathbf{x} . We generated 2,500 sequences with $\tau = 50$ and $\Delta t = 0.02$ and separated them into a training, validation, and test sets with 1,000, 500, and 1,000 sequences, respectively.

⁴We used MLP as the data are fixed length. The same holds hereafter. Extension to other networks is easy.

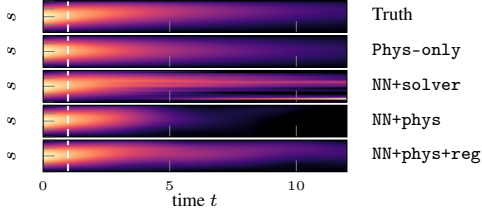


Figure 4: Reconstruction and extrapolation of a test sample of the advection-diffusion data. Range $0 \leq t < 1$ is reconstruction, whereas $t \geq 1$ is extrapolation; dashed line is the border.

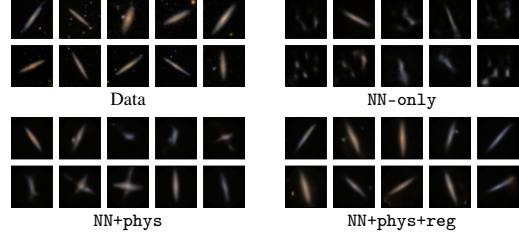


Figure 5: (*upper left*) Subset of the galaxy image data. (*remaining*) Random generation from the learned models.

Setting We set f_P as the diffusion PDE, i.e., $f_P(T, z_P) := \partial T / \partial t - z_P \partial^2 T / \partial s^2$, where $z_P \in \mathbb{R}$ should work as diffusion coefficient a . We augmented it by $f_A(T, z_A)$ additively, where f_A was an MLP and $z_A \in \mathbb{R}^4$. Hence, the decoding process is $\mathcal{F} := \text{solve}_T[f_P(T, z_P) + f_A(T, z_A) = 0]$. We used $h_A = 0$ as the baseline function. The recognition networks, g_A and g_P , were modeled with MLPs. We used the initial snapshot of each sequence x as an estimation of the initial condition T_1 .

Results Figure 4 shows an example of reconstruction with extrapolation. As the training data only comprise sequences of range $0 \leq t < 1$, the remaining range $t \geq 1$ is extrapolation. Only NN+phys+reg (the bottom panel) achieves adequate extrapolation; phys-only lacks advection, NN+solver has unnatural artifacts, and NN+phys infers z_P (i.e., diffusion coefficient a) wrongly.

Table 1 (right half) summarizes the reconstruction and inference errors, which are basically consistent with the results in the pendulum example, in the sense that NN+phys+reg achieves reasonable performance both in reconstruction and inference, while phys-only fails reconstruction, and NN+phys fails inference. Note that the reconstruction performance of NN+phys+reg is slightly worse than some baselines, which is probably due to suboptimal hyperparameters. In fact, with finer tuning of the hyperparameters, NN+phys+reg can achieve the reconstruction error closer to other methods while almost keeping the inference error⁵. We also show the performance of ablations of NN+phys+reg, where either of the regularizers was turned off (i.e., $\alpha = 0$, $\beta = 0$, or $\gamma = 0$). Not surprisingly their performance is worse than the full regularization, especially in terms of the inference error.

5.3 Galaxy images

Dataset We used images of galaxy of the Galaxy10 dataset [49]. We selected the 589 images of the “Disk, Edge-on, No Bulge” class and separated them into training, validation, and test sets with 400, 100, and 89 images, respectively. Each image is of size 69×69 with three channels. We performed data augmentation with random rotation and increased the size of the training set by 20 times.

Setting We set $f_P: \mathbb{R}_{>0}^4 \rightarrow \mathbb{R}^{69 \times 69}$ as an exponential profile of the light distribution of galaxies [see 5, and references therein] whose input is $z_P := [I_0 \ A \ B \ \vartheta]^T \in \mathbb{R}_{>0}^4$. Let $[f_P(z_P)]_{i,j}$ denote the (i, j) -element of the output of f_P . Then, for $1 \leq i, j \leq 69$, $[f_P(z_P)]_{i,j} := I_0 \exp(-r_{i,j})$, where $r_{i,j}^2 := (X_j \cos \vartheta - Y_i \sin \vartheta)^2 / A^2 + (X_j \sin \vartheta + Y_i \cos \vartheta)^2 / B^2$, and (X_j, Y_i) is the coordinate on the 69×69 even grid on $[-1, 1] \times [-1, 1]$. We modify the output of f_P using a U-Net-like neural network $f_A: \mathbb{R}^{69 \times 69} \times \mathbb{R}^{\dim z_A} \rightarrow \mathbb{R}^{69 \times 69 \times 3}$. Thus, the decoding process is $\mathcal{F} := f_A(f_P(z_P), z_A)$. We set $\dim z_A = 2$ for NN+phys+reg. We set $h_A: \mathbb{R}^{69 \times 69} \rightarrow \mathbb{R}^{69 \times 69 \times 3}$ to be the repeat operator along the channel axis. The encoding process is as follows: first, features are extracted from an image x by a convolutional net like [5]. The extracted features are flattened and fed to MLPs g_P and g_A .

⁵In the experiment with the advection-diffusion dataset reported in Table 1, the selected values of the hyperparameters were $\alpha = 0.1$, $\beta = 0.01$, and $\gamma = 10^6$, which were chosen from only eight candidates (see Appendix E for detail). When we instead set $\alpha = 0.032$, $\beta = 0.01$, and $\gamma = 10^6$ in the sensitivity experiment (shown in Appendix F), the reconstruction error of NN+phys+reg was 0.0390 (4.5×10^{-4}), which is comparable to the baselines’ performance in Table 1. In this setting, the inference error of NN+phys+reg was 0.0103 (1.5×10^{-3}). We only reported the suboptimal values in Table 1 to align the granularity of the hyperparameter tuning grid with that in the experiment with the pendulum dataset.

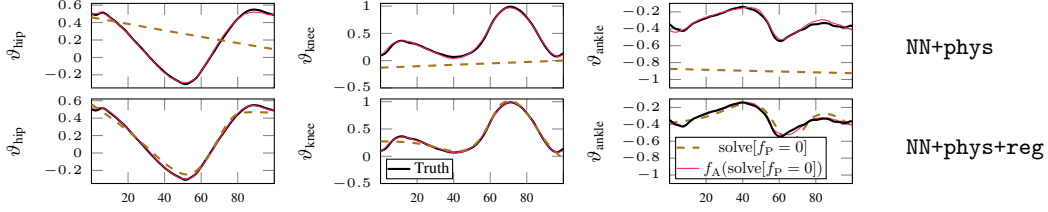


Figure 6: Reconstruction of a test sample of the gait data. Horizontal axis is normalized time.

Results Figure 5 shows an example of original data and random generation from the learned models. NN-only tends to generate non-realistic images, and NN+phys generates slightly better but still spuriously, whereas NN+phys+reg consistently generates galaxy-like images. More results (reconstruction, counterfactual generation, and inspection of latent variable) are deferred to Appendix F.

5.4 Human gait

Dataset We used a part of the dataset provided by [48], which contains measurements of locomotion at different speeds of 50 subjects. We extracted the angles of hip, knee, and ankle in the sagittal plane. Data originally comprise sequences of each stride normalized to be 100 steps, so each data-point x is a sequence $x := [\vartheta_1 \cdots \vartheta_{100}] \in \mathbb{R}^{3 \times 100}$, where $\vartheta_j := [\vartheta_{\text{hip},j} \ \vartheta_{\text{knee},j} \ \vartheta_{\text{ankle},j}]^T$. We used different 400, 100, and 344 sequences as training, validation, and test sets, respectively.

Setting Biomechanical modeling of gait is a long-standing problem [see, e.g., 78]. We did not choose a specific model but let f_P be a trainable Hamilton’s equation as in [91, 29]. $z_P \in \mathbb{R}^{2d_H}$ worked as the initial conditions of it, where d_H was the dimensionality of the generalized position. We let $d_H = 3$ and modeled the neural Hamiltonian with an MLP. The solution of $f_P = 0$ was transformed by f_A that also took $z_A \in \mathbb{R}^{15}$ as an argument. In summary, the decoding process is $\mathcal{F} = f_A(\text{solve}[f_P = 0], z_A)$. We set h_A to be an affine transform at each timestep, which had a weight matrix and a bias as param(h). The recognition networks were modeled with MLPs.

Results Figure 6 is for visually comparing the difference of the learned models’ behavior due to the proposed regularizers. We compare the reconstructions by NN+phys and NN+phys+reg. The dashed lines show an intermediate of the decoding process, i.e., $\text{solve}[f_P = 0]$, and the red solid lines show the final reconstruction, i.e., $f_A(\text{solve}[f_P = 0])$. Without the regularization (upper row), $\text{solve}[f_P = 0]$ returns almost meaningless signals, and f_A bears the most effort of reconstruction. On the other hand, with the regularization (lower row), $\text{solve}[f_P = 0]$ already matches well the data, and f_A modifies it only slightly. Superiority of the regularized model was also confirmed quantitatively; the average test reconstruction errors were 0.273 with NN+phys and 0.259 with NN+phys+reg.

6 Conclusion

Physics-integrated VAEs by construction attain partial interpretability as some of the latent variables are semantically grounded to the physics models, and thus we can generate signals in a controlled manner. Moreover, they have extrapolation capability due to the physics models. In this work, we proposed a regularized learning objective for ensuring a proper functionality of the integrated physics models. We empirically validated the aforementioned unique capability of physics-integrated VAEs and the importance of the proposed regularization method. In future studies, it would be interesting to investigate possibility and extension to learn a hybrid generative model with a highly complex observation process.

Acknowledgments and Disclosure of Funding

This work was supported by the Innosuisse project *Industrial artificial intelligence for intelligent machines and manufacturing digitalization* (39453.1 IP-ICT) and the Swiss National Science Foundation Sinergia project *Modeling pathological gait resulting from motor impairments* (CRSII5_177179).

References

- [1] A. Ajay, J. Wu, N. Fazeli, M. Bauza, L. P. Kaelbling, J. B. Tenenbaum, and A. Rodriguez. Augmenting physical simulators with stochastic neural networks: Case study of planar pushing and bouncing. In *Proceedings of the 2018 IEEE/RSJ International Conference on Intelligent Robots and Systems*, pages 3066–3073, 2018.
- [2] A. Ajay, M. Bauza, J. Wu, N. Fazeli, J. B. Tenenbaum, A. Rodriguez, and L. P. Kaelbling. Combining physical simulators and object-based networks for control. In *Proceedings of the 2019 IEEE International Conference on Robotics and Automation*, pages 3217–3223, 2019.
- [3] M. Álvarez, D. Luengo, and N. D. Lawrence. Latent force models. In *Proceedings of the 12th International Conference on Artificial Intelligence and Statistics*, pages 9–16, 2009.
- [4] B. Amos and J. Z. Kolter. OptNet: Differentiable optimization as a layer in neural networks. In *Proceedings of the 34th International Conference on Machine Learning*, pages 136–145, 2017.
- [5] M. A. Aragon-Calvo and J. C. Carvajal. Self-supervised learning with physics-aware neural networks – I. Galaxy model fitting. *Monthly Notices of the Royal Astronomical Society*, 498(3):3713–3719, 2020.
- [6] S. Ö. Arik, C.-L. Li, J. Yoon, R. Sinha, A. Epshteyn, L. T. Le, V. Menon, S. Singh, L. Zhang, N. Yoder, M. Nikoltchev, Y. Sonthalia, H. Nakhost, E. Kanal, and T. Pfister. Interpretable sequence learning for COVID-19 forecasting. arXiv:2008.00646, 2020.
- [7] Y. Ba, G. Zhao, and A. Kadambi. Blending diverse physical priors with neural networks. arXiv:1910.00201, 2019.
- [8] K. Beckh, S. Müller, M. Jakobs, V. Toborek, H. Tan, R. Fischer, P. Welke, S. Houben, and L. von Rueden. Explainable machine learning with prior knowledge: An overview. arXiv:2105.10172, 2021.
- [9] A. Behjat, C. Zeng, R. Rai, I. Matei, D. Doermann, and S. Chowdhury. A physics-aware learning architecture with input transfer networks for predictive modeling. *Applied Soft Computing*, 96:106665, 2020.
- [10] F. d. A. Belbute-Peres, T. D. Economon, and J. Z. Kolter. Combining differentiable PDE solvers and graph neural networks for fluid flow prediction. In *Proceedings of the 37th International Conference on Machine Learning*, pages 2402–2411, 2020.
- [11] G. Camps-Valls, D. H. Svendsen, J. Cortés-Andrés, Á. Moreno-Martínez, A. Pérez-Suay, J. Adsuara, I. Martín, M. Piles, J. Muñoz-Marí, and L. Martino. Living in the physics and machine learning interplay for earth observation. arXiv:2010.09031, 2020.
- [12] F. P. Casale, A. Dalca, L. Saglietti, J. Listgarten, and N. Fusi. Gaussian process prior variational autoencoders. In *Advances in Neural Information Processing Systems 31*, pages 10369–10380, 2018.
- [13] C. Chen, G. Zheng, H. Wei, and Z. Li. Physics-informed generative adversarial networks for sequence generation with limited data. NeurIPS Workshop on Interpretable Inductive Biases and Physically Structured Learning, 2020.
- [14] T. Q. Chen, Y. Rubanova, J. Bettencourt, and D. K. Duvenaud. Neural ordinary differential equations. In *Advances in Neural Information Processing Systems 31*, pages 6572–6583, 2018.
- [15] X. Chen, X. Xu, X. Liu, S. Pan, J. He, H. Y. Noh, L. Zhang, and P. Zhang. PGA: Physics guided and adaptive approach for mobile fine-grained air pollution estimation. In *Proceedings of the 2018 ACM International Joint Conference on Pervasive and Ubiquitous Computing and Wearable Computers*, pages 1321–1330, 2018.
- [16] J. Chung, K. Kastner, L. Dinh, K. Goel, A. Courville, and Y. Bengio. A recurrent latent variable model for sequential data. In *Advances in Neural Information Processing Systems 28*, pages 2980–2988, 2015.

- [17] K. Cranmer, J. Brehmer, and G. Louppe. The frontier of simulation-based inference. *Proceedings of the National Academy of Sciences*, page 201912789, 2020.
- [18] M. Cranmer, S. Greydanus, S. Hoyer, P. Battaglia, D. Spergel, and S. Ho. Lagrangian neural networks. arXiv:2003.04630, 2020.
- [19] E. de Bézenac, A. Pajot, and P. Gallinari. Deep learning for physical processes: Incorporating prior scientific knowledge. *Journal of Statistical Mechanics: Theory and Experiment*, 2019 (12):124009, 2019.
- [20] W. De Groote, E. Kikken, E. Hostens, S. Van Hoecke, and G. Crevecoeur. Neural network augmented physics models for systems with partially unknown dynamics: Application to slider-crank mechanism. arXiv:1910.12212, 2019.
- [21] M. Déchelle, J. Donà, K. Plessis-Fraissard, P. Gallinari, and M. Levy. Bridging dynamical models and deep networks to solve forward and inverse problems. NeurIPS workshop on Interpretable Inductive Biases and Physically Structured Learning, 2020.
- [22] F. Djeumou, C. Neary, E. Goubault, S. Putot, and U. Topcu. Neural networks with physics-informed architectures and constraints for dynamical systems modeling. arXiv:2109.06407, 2021.
- [23] P. Erwin. Imfit: A fast, flexible new program for astronomical image fitting. *The Astrophysical Journal*, 799(2):226, 2015.
- [24] M. Fraccaro, S. K. Sønderby, U. Paquet, and O. Winther. Sequential neural models with stochastic layers. In *Advances in Neural Information Processing Systems 29*, pages 2199–2207, 2016.
- [25] T. Frerix, D. Kochkov, J. A. Smith, D. Cremers, M. P. Brenner, and S. Hoyer. Variational data assimilation with a learned inverse observation operator. In *Proceedings of the 38th International Conference on Machine Learning*, pages 3449–3458, 2021.
- [26] A. Gelman, J. B. Carlin, H. S. Stern, D. B. Dunson, A. Vehtar, and D. B. Rubin. *Bayesian Data Analysis*. Chapman and Hall/CRC, 3rd edition, 2013.
- [27] T. Golany, D. Freedman, and K. Radinsky. SimGANs: Simulator-based generative adversarial networks for ECG synthesis to improve deep ECG classification. In *Proceedings of the 37th International Conference on Machine Learning*, pages 3597–3606, 2020.
- [28] F. Golemo, P.-Y. Oudeyer, A. A. Taïga, and A. Courville. Sim-to-real transfer with neural-augmented robot simulation. In *Proceedings of the 2nd Conference on Robot Learning*, pages 817–828, 2018.
- [29] S. Greydanus, M. Dzamba, and J. Yosinski. Hamiltonian neural networks. In *Advances in Neural Information Processing Systems 32*, pages 15379–15389, 2019.
- [30] E. Heiden, D. Millard, E. Coumans, Y. Sheng, and G. S. Sukhatme. NeuralSim: Augmenting differentiable simulators with neural networks. arXiv:2011.04217, 2020.
- [31] I. Higgins, L. Matthey, A. Pal, C. Burgess, X. Glorot, M. Botvinick, S. Mohamed, and A. Lerchner. β -VAE: Learning basic visual concepts with a constrained variational framework. In *Proceedings of the 5th International Conference on Learning Representations*, 2017.
- [32] M. Jaques, M. Burke, and T. Hospedales. Physics-as-inverse-graphics: Unsupervised physical parameter estimation from video. In *Proceedings of the 8th International Conference on Learning Representations*, 2020.
- [33] X. Jia, J. Willard, A. Karpatne, J. Read, J. Zwart, M. Steinbach, and V. Kumar. Physics guided RNNs for modeling dynamical systems: A case study in simulating lake temperature profiles. In *Proceedings of the 2019 SIAM International Conference on Data Mining*, pages 558–566, 2019.
- [34] Y. Jiang, J. Sun, and C. K. Liu. Data-augmented contact model for rigid body simulation. arXiv:1803.04019, 2018.

- [35] Y. Jiang, T. Zhang, D. Ho, Y. Bai, C. K. Liu, S. Levine, and J. Tan. SimGAN: Hybrid simulator identification for domain adaptation via adversarial reinforcement learning. arXiv:2101.06005, 2021.
- [36] S. Kaltenbach and P.-S. Koutsourelakis. Incorporating physical constraints in a deep probabilistic machine learning framework for coarse-graining dynamical systems. *Journal of Computational Physics*, 419:109673, 2020.
- [37] S. Kaltenbach and P.-S. Koutsourelakis. Physics-aware, probabilistic model order reduction with guaranteed stability. In *Proceedings of the 9th International Conference on Learning Representations*, 2021.
- [38] M. Karl, M. Soelch, J. Bayer, and P. van der Smagt. Deep variational Bayes filters: Unsupervised learning of state space models from raw data. In *Proceedings of the 5th International Conference on Learning Representations*, 2017.
- [39] G. E. Karniadakis, I. G. Kevrekidis, L. Lu, P. Perdikaris, S. Wang, and L. Yang. Physics-informed machine learning. *Nature Reviews Physics*, 2021.
- [40] A. Karpatne, G. Atluri, J. Faghmous, M. Steinbach, A. Banerjee, A. Ganguly, S. Shekhar, N. Samatova, and V. Kumar. Theory-guided data science: A new paradigm for scientific discovery from data. *IEEE Transactions on Knowledge and Data Engineering*, 29(10):2318–2331, 2017.
- [41] A. Karpatne, W. Watkins, J. Read, and V. Kumar. Physics-guided neural networks (PGNN): An application in lake temperature modeling. arXiv:1710.11431, 2017.
- [42] S. Karra, B. Ahmmed, and M. K. Mudunuru. AdjointNet: Constraining machine learning models with physics-based codes. arXiv:2109.03956, 2021.
- [43] D. P. Kingma and M. Welling. Auto-encoding variational Bayes. In *Proceedings of the 2nd International Conference on Learning Representations*, 2014.
- [44] R. G. Krishnan, U. Shalit, and D. Sontag. Structured inference networks for nonlinear state space models. In *Proceedings of the 31st AAAI Conference on Artificial Intelligence*, pages 2101–2109, 2017.
- [45] F. Lanusse, P. Melchior, and F. Moolekamp. Hybrid physical-deep learning model for astronomical inverse problems. arXiv:1912.03980, 2019.
- [46] V. Le Guen and N. Thome. Disentangling physical dynamics from unknown factors for unsupervised video prediction. In *Proceedings of the 2020 IEEE/CVF Conference on Computer Vision and Pattern Recognition*, pages 11471–11481, 2020.
- [47] F. Leeb, Y. Annadani, S. Bauer, and B. Schölkopf. Structured representation learning using structural autoencoders and hybridization. arXiv:2006.07796, 2021.
- [48] T. Lencioni, I. Carpinella, M. Rabuffetti, A. Marzegan, and M. Ferrarin. Human kinematic, kinetic and EMG data during different walking and stair ascending and descending tasks. *Scientific Data*, 6(1):309, 2019.
- [49] H. W. Leung and J. Bovy. Deep learning of multi-element abundances from high-resolution spectroscopic data. *Monthly Notices of the Royal Astronomical Society*, 483(3):3255–3277, 2018.
- [50] L. Li, S. Hoyer, R. Pederson, R. Sun, E. D. Cubuk, P. Riley, and K. Burke. Kohn-Sham equations as regularizer: Building prior knowledge into machine-learned physics. *Physical Review Letters*, 126(3):036401, 2020.
- [51] Y. Li and S. Mandt. Disentangled sequential autoencoder. In *Proceedings of the 35th International Conference on Machine Learning*, pages 5670–5679, 2018.
- [52] O. Linial, D. Eytan, and U. Shalit. Generative ODE modeling with known unknowns. arXiv:2003.10775, 2020.

- [53] Y. Long and X. She. HybridNet: Integrating model-based and data-driven learning to predict evolution of dynamical systems. In *Proceedings of the 2nd Conference on Robot Learning*, pages 551–560, 2018.
- [54] Z. Long, Y. Lu, X. Ma, and B. Dong. PDE-net: Learning PDEs from data. In *Proceedings of the 35th International Conference on Machine Learning*, pages 3208–3216, 2018.
- [55] Z. Long, Y. Lu, and B. Dong. PDE-Net 2.0: Learning PDEs from data with a numeric-symbolic hybrid deep network. *Journal of Computational Physics*, 399:108925, 2019.
- [56] M. Lutter, C. Ritter, and J. Peters. Deep Lagrangian networks: Using physics as model prior for deep learning. In *Proceedings of the 7th International Conference on Learning Representations*, 2019.
- [57] I. Matei, J. de Kleer, C. Somarakis, R. Rai, and J. S. Baras. Interpretable machine learning models: A physics-based view. arXiv:2003.10025, 2020.
- [58] V. Mehta, I. Char, W. Neiswanger, Y. Chung, A. O. Nelson, M. D. Boyer, E. Kolemen, and J. Schneider. Neural dynamical systems: Balancing structure and flexibility in physical prediction. arXiv:2006.12682, 2020.
- [59] S. K. Mitusch, S. W. Funke, and M. Kuchta. Hybrid FEM-NN models: Combining artificial neural networks with the finite element method. *Journal of Computational Physics*, 446:110651, 2021.
- [60] A. T. Mohan, N. Lubbers, D. Livescu, and M. Chertkov. Embedding hard physical constraints in neural network coarse-graining of 3D turbulence. arXiv:2002.00021, 2020.
- [61] N. Muralidhar, J. Bu, Z. Cao, L. He, N. Ramakrishnan, D. Tafti, and A. Karpatne. PhyNet: Physics guided neural networks for particle drag force prediction in assembly. In *Proceedings of the 2020 SIAM International Conference on Data Mining*, pages 559–567, 2020.
- [62] H. V. Nguyen and T. Bui-Thanh. Model-constrained deep learning approaches for inverse problems. arXiv:2105.12033, 2021.
- [63] A. Nutkiewicz, Z. Yang, and R. K. Jain. Data-driven Urban Energy Simulation (DUE-S): A framework for integrating engineering simulation and machine learning methods in a multi-scale urban energy modeling workflow. *Applied Energy*, 225:1176–1189, 2018.
- [64] S. Pakravan, P. A. Mistani, M. A. Aragon-Calvo, and F. Gibou. Solving inverse-PDE problems with physics-aware neural networks. arXiv:2001.03608, 2020.
- [65] S. Pawar, O. San, B. Aksoylu, A. Rasheed, and T. Kvamsdal. Physics guided machine learning using simplified theories. arXiv:2012.13343, 2020.
- [66] D. Pitchforth, T. Rogers, U. Tygesen, and E. Cross. Grey-box models for wave loading prediction. *Mechanical Systems and Signal Processing*, 159:107741, 2021.
- [67] D. C. Psychogios and L. H. Ungar. A hybrid neural network-first principles approach to process modeling. *AIChE Journal*, 38(10):1499–1511, 1992.
- [68] Z. Qian, W. R. Zame, L. M. Fleuren, P. Elbers, and M. van der Schaar. Integrating expert ODEs into Neural ODEs: Pharmacology and disease progression. arXiv:2106.02875, 2021.
- [69] C. Rackauckas, Y. Ma, J. Martensen, C. Warner, K. Zubov, R. Supekar, D. Skinner, A. Ramadhan, and A. Edelman. Universal differential equations for scientific machine learning. arXiv:2001.04385, 2020.
- [70] M. Raissi. Deep hidden physics models: Deep learning of nonlinear partial differential equations. *Journal of Machine Learning Research*, 19(25):1–24, 2018.
- [71] M. Raissi, P. Perdikaris, and G. E. Karniadakis. Physics-informed neural networks: A deep learning framework for solving forward and inverse problems involving nonlinear partial differential equations. *Journal of Computational Physics*, 378:686–707, 2019.

- [72] M. Reichstein, G. Camps-Valls, B. Stevens, M. Jung, J. Denzler, N. Carvalhais, and Prabhat. Deep learning and process understanding for data-driven Earth system science. *Nature*, 566(7743):195–204, 2019.
- [73] R. Reinhart, Z. Shareef, and J. Steil. Hybrid analytical and data-driven modeling for feed-forward robot control. *Sensors*, 17(2):311, 2017.
- [74] H. Ren, R. Stewart, J. Song, V. Kuleshov, and S. Ermon. Learning with weak supervision from physics and data-driven constraints. *AI Magazine*, 39(1):27–38, 2018.
- [75] D. J. Rezende, S. Mohamed, and D. Wierstra. Stochastic backpropagation and approximate inference in deep generative models. In *Proceedings of the 31st International Conference on Machine Learning*, pages 1278–1286, 2014.
- [76] R. Rico-Martínez, J. S. Anderson, and I. G. Kevrekidis. Continuous-time nonlinear signal processing: A neural network based approach for gray box identification. In *Proceedings of the IEEE Workshop on Neural Networks for Signal Processing*, pages 596–605, 1994.
- [77] M. Rixner and P.-S. Koutsourelakis. A probabilistic generative model for semi-supervised training of coarse-grained surrogates and enforcing physical constraints through virtual observables. arXiv:2006.01789, 2020.
- [78] D. G. E. Robertson, G. E. Caldwell, J. Hamill, G. Kamen, and S. N. Whittlesey. *Research Methods in Biomechanics*. Human Kinetics, 2nd edition, 2014.
- [79] M. A. Roehrl, T. A. Runkler, V. Brandtstetter, M. Tokic, and S. Obermayer. Modeling system dynamics with physics-informed neural networks based on Lagrangian mechanics. arXiv:2005.14617, 2020.
- [80] S. Saemundsson, A. Terenin, K. Hofmann, and M. Deisenroth. Variational integrator networks for physically structured embeddings. In *Proceedings of the 23rd International Conference on Artificial Intelligence and Statistics*, pages 3078–3087, 2020.
- [81] B. Schölkopf, F. Locatello, S. Bauer, N. R. Ke, N. Kalchbrenner, A. Goyal, and Y. Bengio. Towards causal representation learning. arXiv:2102.11107, 2021.
- [82] U. Sengupta, M. Amos, J. S. Hosking, C. E. Rasmussen, M. Juniper, and P. J. Young. Ensembling geophysical models with Bayesian neural networks. In *Advances in Neural Information Processing Systems 33*, 2020.
- [83] N. Shlezinger, J. Whang, Y. C. Eldar, and A. G. Dimakis. Model-based deep learning. arXiv:2012.08405, 2020.
- [84] G. Silvestri, E. Fertig, D. Moore, and L. Ambrogioni. Embedded-model flows: Combining the inductive biases of model-free deep learning and explicit probabilistic modeling. arXiv:2110.06021, 2021.
- [85] S. K. Singh, R. Yang, A. Behjat, R. Rai, S. Chowdhury, and I. Matei. PI-LSTM: Physics-infused long short-term memory network. In *Proceedings of the 18th IEEE International Conference on Machine Learning and Applications*, pages 34–41, 2019.
- [86] R. Stewart and S. Ermon. Label-free supervision of neural networks with physics and domain knowledge. In *Proceedings of the 31st AAAI Conference on Artificial Intelligence*, pages 2576–2582, 2017.
- [87] P. Stinis, T. Hagge, A. M. Tartakovsky, and E. Yeung. Enforcing constraints for interpolation and extrapolation in generative adversarial networks. *Journal of Computational Physics*, 397: 108844, 2019.
- [88] X. Sun, T. Xue, S. M. Rusinkiewicz, and R. P. Adams. Amortized synthesis of constrained configurations using a differentiable surrogate. arXiv:2106.09019, 2021.
- [89] D. J. Tait and T. Damoulas. Variational autoencoding of PDE inverse problems. arXiv:2006.15641, 2020.

- [90] M. L. Thompson and M. A. Kramer. Modeling chemical processes using prior knowledge and neural networks. *AIChE Journal*, 40(8):1328–1340, 1994.
- [91] P. Toth, D. J. Rezende, A. Jaegle, S. Racanière, A. Botev, and I. Higgins. Hamiltonian generative networks. In *Proceedings of the 8th International Conference on Learning Representations*, 2020.
- [92] K. Um, R. Brand, Y. R. Fei, P. Holl, and N. Therey. Solver-in-the-Loop: Learning from differentiable physics to interact with iterative PDE-Solvers. In *Advances in Neural Information Processing Systems 33*, pages 6111–6122, 2020.
- [93] F. A. Viana, R. G. Nascimento, A. Dourado, and Y. A. Yucesan. Estimating model inadequacy in ordinary differential equations with physics-informed neural networks. *Computers & Structures*, 245:106458, 2021.
- [94] L. von Rueden, S. Mayer, K. Beckh, B. Georgiev, S. Giesselbach, R. Heese, B. Kirsch, J. Pfrommer, A. Pick, R. Ramamurthy, M. Walczak, J. Garcke, C. Bauckhage, and J. Schuecker. Informed machine learning – A taxonomy and survey of integrating knowledge into learning systems. arXiv:1903.12394v2, 2020.
- [95] L. von Rueden, S. Mayer, R. Sifa, C. Bauckhage, and J. Garcke. Combining machine learning and simulation to a hybrid modelling approach: Current and future directions. In *Advances in Intelligent Data Analysis XVIII*, number 12080 in Lecture Notes in Computer Science, pages 548–560. 2020.
- [96] Z. Y. Wan, P. Vlachas, P. Koumoutsakos, and T. Sapsis. Data-assisted reduced-order modeling of extreme events in complex dynamical systems. *PLOS ONE*, 13(5):e0197704, 2018.
- [97] Q. Wang, F. Li, Y. Tang, and Y. Xu. Integrating model-driven and data-driven methods for power system frequency stability assessment and control. *IEEE Transactions on Power Systems*, 34(6):4557–4568, 2019.
- [98] S. Wang, Y. Teng, and P. Perdikaris. Understanding and mitigating gradient flow pathologies in physics-informed neural networks. *SIAM Journal on Scientific Computing*, 43(5):A3055–A3081, 2021.
- [99] J. Willard, X. Jia, S. Xu, M. Steinbach, and V. Kumar. Integrating physics-based modeling with machine learning: A survey. arXiv:2003.04919, 2020.
- [100] L. Yang, X. Meng, and G. E. Karniadakis. B-PINNs: Bayesian physics-informed neural networks for forward and inverse PDE problems with noisy data. *Journal of Computational Physics*, 425:109913, 2021.
- [101] Y. Yang and P. Perdikaris. Physics-informed deep generative models. arXiv:1812.03511, 2018.
- [102] Z. Yang, J.-L. Wu, and H. Xiao. Enforcing deterministic constraints on generative adversarial networks for emulating physical systems. arXiv:1911.06671, 2019.
- [103] Ç. Yıldız, M. Heinonen, and H. Lähdesmäki. ODE2VAE: Deep generative second order ODEs with Bayesian neural networks. In *Advances in Neural Information Processing Systems 32*, pages 13412–13421, 2019.
- [104] Y. Yin, V. Le Guen, J. Dona, I. Ayed, E. de Bézenac, N. Thome, and P. Gallinari. Augmenting physical models with deep networks for complex dynamics forecasting. In *Proceedings of the 9th International Conference on Learning Representations*, 2021.
- [105] C.-C. Young, W.-C. Liu, and M.-C. Wu. A physically based and machine learning hybrid approach for accurate rainfall-runoff modeling during extreme typhoon events. *Applied Soft Computing*, 53:205–216, 2017.
- [106] A. Zeng, S. Song, J. Lee, A. Rodriguez, and T. Funkhouser. TossingBot: Learning to throw arbitrary objects with residual physics. In *Proceedings of Robotics: Science and Systems*, 2019.

- [107] J. Zhang, C. Wei, and C. Wu. Thermodynamic consistent neural networks for learning material interfacial mechanics. arXiv:2011.14172, 2020.
- [108] R. Zhang, Y. Liu, and H. Sun. Physics-guided convolutional neural network (PhyCNN) for data-driven seismic response modeling. *Engineering Structures*, 215:110704, 2020.
- [109] Z. Zhang, R. Rai, S. Chowdhury, and D. Doermann. MIDPhyNet: Memorized infusion of decomposed physics in neural networks to model dynamic systems. *Neurocomputing*, 428: 116–129, 2021.
- [110] S. Zhao, J. Song, and S. Ermon. The information autoencoding family: A Lagrangian perspective on latent variable generative models. In *Proceedings of the 34th Conference on Uncertainty in Artificial Intelligence*, 2018.
- [111] S. Zhao, J. Song, and S. Ermon. InfoVAE: Balancing learning and inference in variational autoencoders. In *Proceedings of the 33rd AAAI Conference on Artificial Intelligence*, pages 5885–5892, 2019.

A General description of physics-integrated VAEs

In this section, we provide a general description of the physics-integrated VAEs and the proposed regularization method, since we only described a simple case in Sections 2 and 3 of the main text. The main difference of the general description from the simple one is the number of trainable function f_A in the model.

A.1 Model

We here consider a generalized case in which we have multiple trainable models $f_{A,1}, f_{A,2}, \dots, f_{A,K}$. We fix the number of f_P to be one as in the main text for clarity, while an extension in this regard is straightforward. We exemplify some use cases with multiple f_A 's in Appendix D.

A.1.1 Latent variables

Beside $z_P \in \mathcal{Z}_P$, we consider $z_{A,k} \in \mathcal{Z}_{A,k}$ for $k = 1, \dots, K$. If $f_{A,k}$ does not take z as argument for some k , we simply suppose $\mathcal{Z}_{A,k} = \emptyset$ for such k . Otherwise, we suppose that $\mathcal{Z}_{A,k}$ is (some subset of) the Euclidean space for simplicity of discussion. The prior distributions are:

$$p(z_P) := \mathcal{N}(z_P \mid \mathbf{m}_P, v_P^2 \mathbf{I}), \quad (13)$$

and

$$p(z_{A,k}) := \mathcal{N}(z_{A,k} \mid \mathbf{0}, \mathbf{I}), \quad (14)$$

for k whose $\mathcal{Z}_{A,k}$ is not empty.

A.1.2 Decoder

We intentionally do not specify the ranges and the domains of f_P and $f_{A,1}, f_{A,2}, \dots, f_{A,K}$ because they depend on how these functions are connected each other. We denote the decoding process again with a functional \mathcal{F} whose arguments are f_P and $f_{A,1}, \dots, f_{A,K}$ as well as z 's, that is, $\mathcal{F}[f_P, f_{A,1}, \dots, f_{A,K}; z_P, z_{A,1}, \dots, z_{A,K}]$ ⁶. Inside \mathcal{F} the functions can be connected in various ways; \mathcal{F} can include 1) *in-equation* augmentation $\text{solve}(f_P + f_A = 0)$ or $\text{solve}(f_A \circ f_P = 0)$, 2) *out-equation* augmentation $f_A(\text{solve}(f_P = 0))$, and 3) their arbitrary combinations, e.g., $f_{A,3}(\text{solve}(f_{A,2}(f_P + f_{A,1}) = 0))$. We show some examples in Appendix D. The observation model is

$$p_\theta(\mathbf{x} \mid z_P, z_{A,1}, \dots, z_{A,K}) := \mathcal{N}(\mathbf{x} \mid \mathcal{F}[f_P, f_{A,1}, \dots, f_{A,K}; z_P, z_{A,1}, \dots, z_{A,K}], \Sigma_x), \quad (15)$$

where θ is the set of trainable parameters of f_P and $f_{A,1}, \dots, f_{A,K}$ (and Σ_x).

⁶Note that the expression in Section 2 of the main text, $\mathcal{F}[f_A(f_P(z_P), z_A)]$, violates this general notation; for consistency, it should have been $\mathcal{F}[f_P, f_A; z_P, z_A]$ instead. The idea there was to emphasize the fact that f_A and f_P are *somehow* (not only additively) composited in the model.

A.1.3 Encoder

Accordingly, the approximated posterior is

$$q_\psi(\mathbf{z}_P, \mathbf{z}_{A,1}, \dots, \mathbf{z}_{A,K} | \mathbf{x}) := q_\psi(\mathbf{z}_{A,1}, \dots, \mathbf{z}_{A,K} | \mathbf{x})q_\psi(\mathbf{z}_P | \mathbf{x}, \mathbf{z}_{A,1}, \dots, \mathbf{z}_{A,K}). \quad (16)$$

We do not specify further structures of $q_\psi(\mathbf{z}_{A,1}, \dots, \mathbf{z}_{A,K} | \mathbf{x})$ and $q_\psi(\mathbf{z}_P | \mathbf{x}, \mathbf{z}_{A,1}, \dots, \mathbf{z}_{A,K})$ because they depend on use cases. We denote the recognition networks for \mathbf{z}_P and $\mathbf{z}_{A,k}$ by g_P and $g_{A,k}$, respectively for $k = 1, \dots, K$. ψ is again the set of all the trainable parameters in the encoder side of the model.

A.2 Regularizers

We slightly modify the definition of the proposed regularizers in accordance with the general description of the model.

The regularizer to suppress trainable components, R_{PPC} , should be able to measure the contribution of all the trainable components, $f_{A,1}, \dots, f_{A,K}$. While the original definition in Section 3 of the main text would still work as is, we empirically found that the following modification was useful in some cases. The idea is to consider the *marginal contribution* (compared to the physics model) of *each* of the trainable components, $f_{A,1}, \dots, f_{A,K}$, instead of computing the contribution of all f_A 's altogether. To show the essence of the idea, let us suppose $K = 2$. We consider the discrepancy between posterior predictive distributions for the following combinations:

$$D_{\text{KL}}[p_{\theta,\psi}(\tilde{\mathbf{x}} | X) \parallel p_{\theta^r,\psi}^{\text{r},\{1\}}(\tilde{\mathbf{x}} | X)], \quad (17)$$

$$D_{\text{KL}}[p_{\theta,\psi}(\tilde{\mathbf{x}} | X) \parallel p_{\theta^r,\psi}^{\text{r},\{2\}}(\tilde{\mathbf{x}} | X)], \quad (18)$$

$$D_{\text{KL}}[p_{\theta^r,\psi}^{\text{r},\{1\}}(\tilde{\mathbf{x}} | X) \parallel p_{\theta^r,\psi}^{\text{r},\{1,2\}}(\tilde{\mathbf{x}} | X)], \quad (19)$$

$$D_{\text{KL}}[p_{\theta^r,\psi}^{\text{r},\{2\}}(\tilde{\mathbf{x}} | X) \parallel p_{\theta^r,\psi}^{\text{r},\{1,2\}}(\tilde{\mathbf{x}} | X)], \quad (20)$$

where $p_{\theta^r,\psi}^{\text{r},\mathcal{I}}(\tilde{\mathbf{x}} | X)$ ($\mathcal{I} \subseteq \{1, \dots, K\}$) is a *partial* physics-only reduced model in which $f_{A,i}, \forall i \in \mathcal{I}$ are replaced with baseline function $h_{A,i}$. We let $p_{\theta^r,\psi}^{\text{r},\mathcal{I}=\emptyset}(\tilde{\mathbf{x}} | X) := p_{\theta,\psi}(\tilde{\mathbf{x}} | X)$ for convenience of notation.

Let us denote the upper bounds (see Proposition 1) of Eqs. (17)–(20) respectively as follows:

$$\begin{aligned} & \mathbb{E}_{p_d(\mathbf{x}|X)} \hat{D}_{\emptyset,\{1\}}(\theta, \text{param}(h), \psi; \mathbf{x}), \\ & \mathbb{E}_{p_d(\mathbf{x}|X)} \hat{D}_{\emptyset,\{2\}}(\theta, \text{param}(h), \psi; \mathbf{x}), \\ & \mathbb{E}_{p_d(\mathbf{x}|X)} \hat{D}_{\{1\},\{1,2\}}(\theta, \text{param}(h), \psi; \mathbf{x}), \\ & \mathbb{E}_{p_d(\mathbf{x}|X)} \hat{D}_{\{2\},\{1,2\}}(\theta, \text{param}(h), \psi; \mathbf{x}). \end{aligned}$$

Then, the regularizer is defined as

$$\begin{aligned} & 4R_{\text{PPC}}(\theta, \text{param}(h), \psi) \\ & := \mathbb{E}_{p_d(\mathbf{x}|X)} \hat{D}_{\emptyset,\{1\}}(\theta, \text{param}(h), \psi; \mathbf{x}) + \mathbb{E}_{p_d(\mathbf{x}|X)} \hat{D}_{\emptyset,\{2\}}(\theta, \text{param}(h), \psi; \mathbf{x}) \\ & \quad + \mathbb{E}_{p_d(\mathbf{x}|X)} \hat{D}_{\{1\},\{1,2\}}(\theta, \text{param}(h), \psi; \mathbf{x}) + \mathbb{E}_{p_d(\mathbf{x}|X)} \hat{D}_{\{2\},\{1,2\}}(\theta, \text{param}(h), \psi; \mathbf{x}). \end{aligned} \quad (21)$$

The regularizer to use physics-based data augmentation, R_{DA} , is defined in almost the same way as in the simple case — we draw samples \mathbf{z}_P^* from some distribution of \mathbf{z}_P and generate physics-only augmentation by $\mathbf{x}^r(\mathbf{z}_P^*) := \mathcal{F}[f_P, h_{A,1}, \dots, h_{A,K}; \mathbf{z}_P^*]$. Note that all of f_A 's are replaced with h_A 's at once unlike the aforementioned case of R_{PPC} .

B Proof of Proposition 1

We use the following well-known facts in deriving the upper bound in Proposition 1.

Lemma 1. *Let $p_1(x, y)$ and $p_2(x, y)$ be two joint distributions on random variables x and y , and $p_1(x)$ and $p_2(x)$ be the corresponding marginals. Then,*

$$D_{\text{KL}}[p_1(x) \parallel p_2(x)] \leq D_{\text{KL}}[p_1(x, y) \parallel p_2(x, y)]. \quad (22)$$

Proof. From definition,

$$\begin{aligned}
D_{\text{KL}}[p_1(x, y) \parallel p_2(x, y)] &= \int p_1(x, y) \frac{p_1(x, y)}{p_2(x, y)} dx dy \\
&= \int p_1(y | x) p_1(x) \frac{p_1(y | x) p_1(x)}{p_2(y | x) p_2(x)} dx dy \\
&= \int p_1(y | x) p_1(x) \frac{p_1(y | x)}{p_2(y | x)} dx dy + \int p_1(y | x) p_1(x) \frac{p_1(x)}{p_2(x)} dx dy \\
&= \int p_1(x) \left(\int p_1(y | x) \frac{p_1(y | x)}{p_2(y | x)} dy \right) dx + \int p_1(x) \frac{p_1(x)}{p_2(x)} dx \\
&= \mathbb{E}_{p_1(x)} D_{\text{KL}}[p_1(y | x) \parallel p_2(y | x)] + D_{\text{KL}}[p_1(x) \parallel p_2(x)].
\end{aligned}$$

Hence, from the nonnegativity of the KL divergence, we have

$$\begin{aligned}
D_{\text{KL}}[p_1(x) \parallel p_2(x)] &= D_{\text{KL}}[p_1(x, y) \parallel p_2(x, y)] - \mathbb{E}_{p_1(x)} D_{\text{KL}}[p_1(y | x) \parallel p_2(y | x)] \\
&\leq D_{\text{KL}}[p_1(x, y) \parallel p_2(x, y)].
\end{aligned}$$

□

Lemma 2. Let x and y be random variables with joint distribution $q(x, y)$. Let $I(x; y)$ be the mutual information between x and y , i.e.: $I(x; y) := D_{\text{KL}}[q(x, y) \parallel q(x)q(y)]$. Let $p(x)$ be some distribution of x . Then,

$$I(x; y) \leq \mathbb{E}_{q(y)} D_{\text{KL}}[q(x | y) \parallel p(x)]. \quad (23)$$

Proof. From the nonnegativity of the KL divergence,

$$\begin{aligned}
I(x, y) &= D_{\text{KL}}[q(x, y) \parallel q(x)q(y)] \\
&= \int q(x, y) \log \frac{q(x, y)}{q(x)q(y)} dx dy \\
&= \int q(x, y) \log \frac{q(x | y)}{q(x)} dx dy \\
&= \int q(x, y) \log \frac{q(x | y)p(x)}{p(x)q(x)} dx dy \\
&= \mathbb{E}_{q(y)} D_{\text{KL}}[q(x | y) \parallel p(x)] - D_{\text{KL}}[q(x) \parallel p(x)] \\
&\leq \mathbb{E}_{q(y)} D_{\text{KL}}[q(x | y) \parallel p(x)].
\end{aligned}$$

□

Now we give a proof of Proposition 1.

Proof of Proposition 1. Let us denote the set of \mathbf{z}_P and \mathbf{z}_A by z . As a posterior predictive distribution $p(\tilde{\mathbf{x}} | X)$ is obtained by marginalizing out z and \mathbf{x} of joint distribution $p(\tilde{\mathbf{x}}, z, \mathbf{x} | X)$, from (22),

$$D_{\text{KL}}[p_{\theta, \psi}(\tilde{\mathbf{x}} | X) \parallel p_{\theta^r, \psi}^r(\tilde{\mathbf{x}} | X)] \leq D_{\text{KL}}[p_{\theta, \psi}(\tilde{\mathbf{x}}, z, \mathbf{x} | X) \parallel p_{\theta^r, \psi}^r(\tilde{\mathbf{x}}, z, \mathbf{x} | X)]. \quad (24)$$

The right-hand side of (24) is

$$\begin{aligned}
&D_{\text{KL}}[p_{\theta, \psi}(\tilde{\mathbf{x}}, z, \mathbf{x} | X) \parallel p_{\theta^r, \psi}^r(\tilde{\mathbf{x}}, z, \mathbf{x} | X)] \\
&= D_{\text{KL}}\left[p_{\theta}(\tilde{\mathbf{x}} | z) q_{\psi}(z | \mathbf{x}) p_d(\mathbf{x} | X) \parallel p_{\theta^r}^r(\tilde{\mathbf{x}} | z) q_{\psi}^r(z | \mathbf{x}) p_d(\mathbf{x} | X)\right] \\
&= \mathbb{E}_{p_d(\mathbf{x} | X)} \mathbb{E}_{q_{\psi}(z | \mathbf{x})} D_{\text{KL}}[p_{\theta}(\tilde{\mathbf{x}} | z) \parallel p_{\theta^r}^r(\tilde{\mathbf{x}} | z)] + \mathbb{E}_{p_d(\mathbf{x} | X)} D_{\text{KL}}[q_{\psi}(z | \mathbf{x}) \parallel q_{\psi}^r(z | \mathbf{x})],
\end{aligned}$$

where the last term is

$$\begin{aligned}
&\mathbb{E}_{p_d(\mathbf{x} | X)} D_{\text{KL}}[q_{\psi}(z | \mathbf{x}) \parallel q_{\psi}^r(z | \mathbf{x})] \\
&= \mathbb{E}_{p_d(\mathbf{x} | X)} D_{\text{KL}}[q_{\psi}(\mathbf{z}_P | \mathbf{x}, \mathbf{z}_A) q_{\psi}(\mathbf{z}_A | \mathbf{x}) \parallel q_{\psi}(\mathbf{z}_P | \mathbf{x}) p(\mathbf{z}_A)] \\
&= \mathbb{E}_{p_d(\mathbf{x} | X)} \left[\mathbb{E}_{q_{\psi}(\mathbf{z}_A | \mathbf{x})} D_{\text{KL}}[q_{\psi}(\mathbf{z}_P | \mathbf{x}, \mathbf{z}_A) \parallel q_{\psi}(\mathbf{z}_P | \mathbf{x})] + D_{\text{KL}}[q_{\psi}(\mathbf{z}_A | \mathbf{x}) \parallel p(\mathbf{z}_A)] \right] \\
&= \mathbb{E}_{p_d(\mathbf{x} | X)} \left[I(\mathbf{z}_P; \mathbf{z}_A) + D_{\text{KL}}[q_{\psi}(\mathbf{z}_A | \mathbf{x}) \parallel p(\mathbf{z}_A)] \right].
\end{aligned}$$

Hence, from the upper bound of mutual information, (23), the right-hand side of (24) is further upper bounded as

$$\begin{aligned} & D_{\text{KL}}[p_{\theta,\psi}(\tilde{\mathbf{x}}, z, \mathbf{x} \mid X) \parallel p_{\theta^r,\psi}^r(\tilde{\mathbf{x}}, z, \mathbf{x} \mid X)] \\ & \leq \mathbb{E}_{p_{\text{d}}(\mathbf{x} \mid X)} \left[\mathbb{E}_{q_{\psi}(z \mid \mathbf{x})} D_{\text{KL}}[p_{\theta}(\tilde{\mathbf{x}} \mid z) \parallel p_{\theta^r}^r(\tilde{\mathbf{x}} \mid \mathbf{z}_{\text{P}}, \mathbf{z}_{\text{A}})] \right. \\ & \quad \left. + \mathbb{E}_{q_{\psi}(\mathbf{z}_{\text{A}} \mid \mathbf{x})} D_{\text{KL}}[q_{\psi}(\mathbf{z}_{\text{P}} \mid \mathbf{x}, \mathbf{z}_{\text{A}}) \parallel p(\mathbf{z}_{\text{P}})] + D_{\text{KL}}[q_{\psi}(\mathbf{z}_{\text{A}} \mid \mathbf{x}) \parallel p(\mathbf{z}_{\text{A}})] \right]. \end{aligned}$$

□

C Additional remarks on the regularized learning method

Upper bound of KL in general case In the general case of Appendix A, the upper bound of the KL divergence used for defining R_{PC} becomes slightly different. For example, a bound of (17) is as follows (recall that we focused the case of $K = 2$ for discussion):

$$\begin{aligned} & D_{\text{KL}}[p_{\theta,\psi}(\tilde{\mathbf{x}} \mid X) \parallel p_{\theta^r,\psi}^{r,\{1\}}(\tilde{\mathbf{x}} \mid X)] \leq \mathbb{E}_{p_{\text{d}}(\mathbf{x} \mid X)} \left[\mathbb{E}_{q_{\psi}(\mathbf{z}_{\text{P}}, \mathbf{z}_{\text{A}} \mid \mathbf{x})} D_{\text{KL}}[p_{\theta} \parallel p_{\theta^r}^{r,\{1\}}] \right. \\ & \quad \left. + D_{\text{KL}}[q_{\psi}(\mathbf{z}_{\text{A},1}, \mathbf{z}_{\text{A},2} \mid \mathbf{x}) \parallel p_{\text{A},\{1,2\}}] + \mathbb{E}_{q_{\psi}(\mathbf{z}_{\text{A},1}, \mathbf{z}_{\text{A},2} \mid \mathbf{x})} D_{\text{KL}}[q_{\psi}(\mathbf{z}_{\text{P}} \mid \mathbf{z}_{\text{A},1}, \mathbf{z}_{\text{A},2}, \mathbf{x}) \parallel p_{\text{P}}] \right], \end{aligned}$$

where $p_{\text{A},\{1,2\}}$ is some distribution of $\mathbf{z}_{\text{A},1}$ and $\mathbf{z}_{\text{A},2}$, for example $p_{\text{A},\{1,2\}} = p(\mathbf{z}_{\text{A},1})p(\mathbf{z}_{\text{A},2})$ using priors. This upper bound can be derived analogously to Proposition 1.

Interpretation of upper bound It is interesting that the mutual information $I(\mathbf{z}_{\text{P}}; \mathbf{z}_{\text{A}})$ appears in the intermediate bound of $D_{\text{KL}}[p_{\theta,\psi}(\tilde{\mathbf{x}} \mid X) \parallel p_{\theta^r,\psi}^r(\tilde{\mathbf{x}} \mid X)]$ (see the proof of Proposition 1). Such a mutual information becomes a conditional mutual information (e.g., $I(\mathbf{z}_{\text{P}}; \mathbf{z}_{\text{A},1} \mid \mathbf{z}_{\text{A},2})$) in the general case. Moreover, the last two terms of the upper bound in Proposition 1 are the same as the last two terms of the ELBO when p_{P} and p_{A} are the priors. In such a case, adding them as regularizers to the objective is equivalent to what is done in β -VAE [31]. It would also be interesting to discuss connection with the work by Zhao et al. [110].

Usage of augmented data Data augmented with physics-based prior knowledge can also be used for pretraining (e.g., Jia et al. [33]). We rather generate and use them during the main training procedure as regularizers because the effects of pretraining may diminish in the main training.

D Related work

We introduce related studies that could not be in Section 4 of the main text due to length limit. Recall that in Section 4, we reviewed the studies with the following two perspectives: ‘‘Physics+ML in model design’’ and ‘‘Physics+ML in objective design.’’ In this appendix, we follow a slightly different taxonomy: 1) *physics-integrated*, 2) *physics-informed*, and 3) *physics-inspired* methods. The first two of these three roughly correspond to the two perspectives in Section 4 of the main text. In contrast, we did not focus on the last one, physics-inspired method, in Section 4, while it will be informative for readers to provide a broader view of the context. We refer to some reviews and surveys on these topics, such as ones by Willard et al. [99], von Rueden et al. [94], von Rueden et al. [95], Beckh et al. [8], and Karniadakis et al. [39]. We would like to emphasize that the aforementioned three areas of research are never exclusive, and study that can bridge and unify them will be important.

D.1 Physics-integrated methods

We refer to methods where the model is a combination of physics models and machine learning models as *physics-integrated*⁷ ones. As such an approach was already explained to some extent in Section 4 of the main text, we here focus on exemplifying architectures of physics-integrated models. Most of the studies referred to here did not aim generative modeling originally, though the ideas can be fitted to our general architecture of physics-integrated VAEs. For more information, we recommend consulting the excellent survey / overview papers [e.g., 90, 40, 74, 72, 97, 11, 83, 99, 81].

⁷Though this has been traditionally known as gray-box modeling, here we put an emphasis on the focus on physics-based models and adjust the wording with other related perspectives.

In-equation augmentation A numerical solver of dynamics models such as ODEs, PDEs, and discrete-time difference equations are one of the most prevailing forms of an equation-solving process that can be in a physics-integrated VAE. In such cases, f_P and/or f_A would give terms that appear in a dynamics equation. They are combined additively in many cases [76, 90, 73, 28, 58, 21, 79, 46, 104, 93, 59, 68], for example:

$$\mathcal{F} := \text{solve}_y [f_P(y, z_P) + f_A(y, z_A) = 0], \quad (25)$$

where solve_y refers to a numerical ODE/PDE solver with regard to y and returns the value of the solution on some time/space grid. Another way of combining f_P and f_A in this context is composition [67, 90, 53, 96, 45, 19, 60, 57, 9, 6, 50, 35, 42, 22], for example:

$$\mathcal{F} := \text{solve}_y [f_P(y, z_P, f_A(y, z_A)) = 0], \quad (26)$$

where f_A often gives estimation of some unknown or varying physics parameters in f_P . The order of the composition may reverse [recent examples include 1, 2], that is,

$$\mathcal{F} := \text{solve}_y [f_A(y, z_A, f_P(y, z_P)) = 0], \quad (27)$$

where the output of a physics model is augmented by a machine learning model. Such a mechanism is often called *residual physics*. Some studies consider more complex combinations of f_P and f_A , for example, $\mathcal{F} := \text{solve}[f_{P,2}(f_A(f_{P,1})) = 0]$ [70, 20, 30, 37]. A trickier case appears in Jiang et al. [34], where discrete state of contact dynamics is first determined by a data-driven classifier, which is then used for choosing one of physics models (also including trainable ones) to be used. Moreover, Um et al. [92] considered to correct numerical errors by neural nets inside a differentiable solver of differential equations.

The equation-solving process can be anything else than an ODE/PDE solver. If (augmented) physics models are algebraic equations with closed-form solutions, \mathcal{F} just evaluates some functions [e.g., 5]. If no closed-form solution is available, a differentiable optimizer may be utilized in \mathcal{F} .

We also note that the latent force models [3] are known as a principled method to incorporate physics models in differential equations into Gaussian processes.

Out-equation augmentation Physics and machine learning integration can also happen outside an equation-solving process. The simplest case is

$$\mathcal{F} := f_A(\text{solve}[\dots], z_A) \quad \text{or} \quad \mathcal{F} := f_A(\text{solve}[\dots], z_A) + \text{solve}[\dots], \quad (28)$$

where $\text{solve}[\dots]$ denotes the output of some equation-solving process, which also includes f_P as well as another set of f_A 's. For example, such architectures can be found in the following use cases:

- f_A corrects the output of an equation-solving process, $\text{solve}[\dots]$, to compensate inaccuracy of physics models or unmodeled phenomena [105, 15, 63, 85, 97, 106, 66]. This can also be seen as residual physics.
- f_A works as an observation function that changes signal's modality [29, 56, 103, 52, 91, 18, 80, 32].
- Output of $\text{solve}[\dots]$ is used as input features of machine learning model f_A [41, 65, 61, 109, 10, 66].

In [82], f_A works as the weight of ensemble of physics models, that is,

$$\mathcal{F} := \sum_i f_{A,i}(z_{A,i}) \cdot \text{solve}[\dots]_i. \quad (29)$$

Inverse problems as (VAE) The idea of (Bayesian) inverse problems is in line with the auto-encoding variational Bayes; in inverse problems, the forward process (i.e., a decoder) is known and a corresponding backward process (i.e., an encoder) is to be estimated. For example, Tait and Damoulas [89] propose a VAE whose decoder has a structure based on the finite element method for PDEs. Aragon-Calvo and Carvajal [5] replace VAE's decoder with a light distribution model of galaxies for inferring parameters of galaxy from images. Pakravan et al. [64] integrate a PDE solver into the decoder of a VAE. Nguyen and Bui-Thanh [62] discuss the form of solution for a special case where physics and VAEs are with linear models. Sun et al. [88] use learned surrogate models as the decoder of autoencoders. Similar problems are also discussed in the context of data assimilation [see, e.g., 25] and likelihood-free inference [see, e.g., 17].

D.2 Physics-informed methods

We already introduced some studies in this direction, i.e., designing learning objective based on physics knowledge, in Section 4 of the main text. We call such an approach *physics-informed* after the work of Raissi et al. [71]. As it is not our main interest in this paper, we do not repeat the contents of Section 4; please refer to Section 4, and we also recommend consulting survey papers such as [39]. The study by Wang et al. [98] is also notable here as they analyze the difficulty of training physics-informed neural networks and propose a remedy.

D.3 Physics-inspired methods

While the main interest of this work is integration of *application-specific* physics models into machine learning models, it is worth noting that there are lines of studies where the aim is to design models on the basis of *abstract and general* knowledge of data-generating process. The extent of the abstraction is diverse; in some studies, it is still natural to refer to the utilized knowledge as physics-related (in a narrow sense, i.e., as one of scientific disciplines) [16, 24, 38, 44, 51, 54, 55, 103, 46, 108], and in some other studies, the level of abstraction goes beyond that, e.g., a general model that can realize structural causal models is incorporated [47]. Hence, the heading of this subsection, *physics-inspired*, may not be perfect; we stick to it just for the consistency with the other perspectives.

For example, researchers have been investigating structured generative models for sequential data, in which the structure of latent variables reflects the sequential nature of data [16, 24, 38, 44, 51]. Moreover, Casale et al. [12] proposed to place a Gaussian process prior in VAEs. Note that these studies are never exclusive with the interest of our work and related ones; for example, the VAEs with sequential structures are indeed closely related to the VAEs with ODEs/PDEs [e.g., 103, 54, 55, 46, 108], since only the major difference is whether time is discrete or continuous. The techniques of the structured latent variable models would also be useful in physics-inspired and physics-integrated methods.

E Detailed experimental settings

E.1 Infrastructure

We implemented the models using Python 3.8.0 with PyTorch 1.7.0 and NumPy 1.19.2 throughout the experiments. We used SciPy of version 1.5.2 in generating the synthetic datasets. The computation was performed with a machine equipped with an NVIDIA[®] Tesla[™] V100 GPU in the experiment on the galaxy images dataset. We used a machine equipped with a CPU of Intel[®] Xeon[®] Gold 6148 in the other experiments.

E.2 Forced damped pendulum

Data-generating process We consider a gravity pendulum with damping effect and external force. Let $\vartheta(t)$ be the angle of the pendulum at time t . We generated the data by numerically integrating an ODE:

$$\frac{d^2\vartheta(t)}{dt^2} + \omega^2 \sin \vartheta(t) + \xi \frac{d\vartheta(t)}{dt} - A\omega^2 \cos(2\pi\phi t) = 0,$$

using `scipy.integrate.solve_ivp` with the explicit Runge–Kutta method of order 8. The tolerance parameters `rtol` and `atol` were kept to be the default values, 10^{-3} and 10^{-6} , respectively. We evaluated the solution’s values at timesteps $t = 0, \Delta t, \dots, (\tau - 1)\Delta t$ with $\Delta t = 0.05$ and $\tau = 50$ using the 7-th order interpolation polynomial. The values of the parameters, ω , ξ , A , and ϕ , as well as the initial condition $\vartheta(0)$ were randomly sampled when creating each sequence. The random sampling was with the uniform distributions on the following ranges: $\omega \in [0.785, 3.14]$, $\xi \in [0, 0.8]$, $f \in [3.14, 6.28]$, $A \in [0, 40]$, and $\vartheta(0) \in [-1.57, 1.57]$. The initial condition of $\vartheta(0)$ was fixed to be 0. Each element of each generated sequence was added by zero-mean Gaussian noise with standard deviation 0.01.

Data property The overall dataset we generated comprises 3,500 elements (data-points) in total. Each data-point \mathbf{x} is a sequence of length τ of pendulum’s angle, that is,

$$\mathbf{x}_i := [\vartheta_i(0) \ \vartheta_i(\Delta t) \ \dots \ \vartheta_i((\tau - 1)\Delta t)]^T \in \mathbb{R}^\tau,$$

where $i = 1, \dots, 3500$ is the sample index.

Train/valid/test split We first extracted 500 and 1,000 sequences randomly from the overall dataset as the validation set and the test set, respectively. We then selected 1,000 sequences out of the remaining 2,000 sequences to make a training set. This selection was randomly done every time; so a different random seed resulted in a different training set.

Physics model A part of the data-generating process was given as physics model: $f_P(\vartheta, z_P) := \ddot{\vartheta} + z_P \sin \vartheta$.

Latent variables By construction of f_P , $z_P \in \mathbb{R}$ is expected to work in the same manner as ω in the data-generating process. There were also $z_{A,1} \in \mathbb{R}$ and $z_{A,2} \in \mathbb{R}^2$ in the full NN+phys and NN+phys+reg models. Meanwhile, we used $z_{A,2} \in \mathbb{R}^4$ (and no $z_{A,1}, z_P$) in the NN-only; and $z_{A,1} \in \mathbb{R}^2$ and $z_{A,2} \in \mathbb{R}^2$ (and no z_P) in the NN+solver model.

Decoder architecture We describe the decoder architecture of the full NN+phys and NN+phys+reg models. In the first stage, an ODE $f_P(\vartheta, z_P) + f_{A,1}(\vartheta, z_{A,1}) = 0$ is numerically solved with the Euler method for length τ with step size Δt . Let $\nu \in \mathbb{R}^\tau$ be the solution sequence. In the second stage, ν is then augmented by $f_{A,2}$, i.e., $f_{A,2}(\nu, z_{A,2})$. We modeled $f_{A,1}$ with a multilayer perceptron (MLP) with two hidden layers of size 64. We modeled $f_{A,2}$ also with an MLP with two hidden layers of size 128. We used the exponential linear unit (ELU) with its⁸ $\alpha = 1.0$ as activation function after the hidden layers.

Encoder architecture We describe the encoder architecture of the full NN+phys and NN+phys+reg models. We modeled the recognition networks, $g_{A,1}, g_{A,2}$, and $g_{P,2}$ with MLPs with five hidden layers of size 128, 128, 256, 64, and 32. We modeled $g_{P,1}$ as $g_{P,1}(\mathbf{x}, z_{A,1}, z_{A,2}) = \mathbf{x} + U(\mathbf{x}, z_{A,1}, z_{A,2})$, where U was an MLP with two hidden layers of size 128. We used ELU with its⁸ $\alpha = 1.0$ as activation function after the hidden layers. We put a softplus function after the final output of g_P to make its output positive-valued.

Replacement functions To create the reduced models, we replaced $f_{A,1}$ and $f_{A,2}$ respectively by $h_{A,1} = 0$ and $h_{A,2} = \text{Id}$.

Hyperparameters We selected the hyperparameters, α, β , and γ , from the following sets: $\alpha \in \{10^{-3}, 10^{-2}, 10^{-1}\}$, $\beta \in \{10^{-4}, 10^{-3}, 10^{-2}\}$, and $\gamma \in \{10^{-2}, 10^{-1}, 1\}$. These ranges were chosen to roughly adjust the values of the corresponding regularizers to that of the ELBO. The configuration that achieved the best reconstruction error on the validation set was selected finally: $\alpha = 10^{-2}$, $\beta = 10^{-3}$, and $\gamma = 10^{-1}$. In computing $R_{DA,2}$, we sampled z_P^* from the uniform distribution on range $[0.392, 3.53]$.

Optimization We used the Adam optimizer with its⁹ $\alpha = 10^{-3}$, $\gamma_1 = 0.9$, $\gamma_2 = 0.999$, and $\epsilon = 10^{-3}$. We ran iterations with mini-batch size 200 for 5000 epochs (i.e., 25,000 iterations in total) and saved the model that achieved the best validation reconstruction error.

E.3 Advection-diffusion system

Data-generating process We consider the advection (convection) and diffusion of something (e.g., heat) on the 1-dimensional space, which is described by the following PDE:

$$\frac{\partial T(t, s)}{\partial t} - a \frac{\partial^2 T(t, s)}{\partial s^2} + b \frac{\partial T(t, s)}{\partial s} = 0,$$

where t and s denote the time and space dimension, respectively. We numerically solved this PDE using `scipy.integrate.solve_ivp` with the explicit Runge–Kutta method of order 8. The spatial derivative was computed with discretization on the H -point even grid between $s = 0$ and $s = s_{\max}$ with $H = 12$ and $s_{\max} = 2$. We evaluated the solutions values at timesteps $t = 0, \Delta t, \dots, (\tau - 1)\Delta t$

⁸ α here is different from one of the hyperparameters of the proposed regularizers.

⁹ α and γ here are different from the ones of the hyperparameters of the proposed regularizers.

with $\Delta t = 0.02$ and $\tau = 50$. The initial condition was set $T(0, s) = c \sin(\pi s / s_{\max})$, and we set the Dirichlet boundary condition $T(t, 0) = T(t, s_{\max}) = 0$. The values of the parameters a , b , and c were randomly sampled when creating each sequence. The random sampling was with the uniform distributions on the following ranges: $a \in [10^{-2}, 10^{-1}]$, $b \in [10^{-2}, 10^{-1}]$, and $c \in [0.5, 1.5]$. Each element of each generated sequence was added by zero-mean Gaussian noise with standard deviation 0.001.

Data property The overall dataset we generated comprises 3,500 sequences, each of which is

$$\mathbf{x}_i := \begin{bmatrix} T_i(0, 0) & T_i(\Delta t, 0) & \cdots & T_i((\tau - 1)\Delta t, 0) \\ \vdots & \vdots & & \vdots \\ T_i(0, s_{\max}) & T_i(\Delta t, s_{\max}) & \cdots & T_i((\tau - 1)\Delta t, s_{\max}) \end{bmatrix} \in \mathbb{R}^{H \times \tau}.$$

Train/valid/test split We first extracted 500 and 1,000 sequences randomly from the overall dataset as the validation set and the test set, respectively. We then selected 1,000 sequences out of the remaining 2,000 sequences to make a training set. This selection was randomly done every time; so a different random seed resulted in a different training set.

Physics model A part of the data-generating process was given as physics model: $f_P(T, z_P) := T_t - z_P T_{ss}$.

Latent variables By construction of f_P , $z_P \in \mathbb{R}$ is expected to work in the same manner as a in the data-generating process. There was also $z_A \in \mathbb{R}^4$ in the full NN+phys and NN+phys+reg models. Meanwhile, we used $z_A \in \mathbb{R}^5$ (and no z_P) in the NN-only and NN+solver models.

Decoder architecture We describe the decoder architecture of the full NN+phys and NN+phys+reg models. In \mathcal{F} , a PDE $f_P(T, z_P) + f_A = 0$ was numerically solved with the finite difference method with the explicit scheme for length τ with temporal step size Δt . We modeled f_A with an MLP with two hidden layers of size 64. We used ELU with its⁸ $\alpha = 1.0$ as activation function after the hidden layers. In the NN-only model, we modeled f_A with an MLP with a hidden layer of size 128.

Encoder architecture We describe the encoder architecture of the full NN+phys and NN+phys+reg models. We modeled the recognition networks, g_A and $g_{P,2}$, with MLPs with five hidden layers of size 256, 256, 256, 64, and 32. We modeled $g_{P,1}(x, z_A)$ with an MLP with two hidden layers of size 256. We used ELU with its⁸ $\alpha = 1.0$ as activation function after the hidden layers. We put a softplus function after the final output of g_P to make its output positive-valued.

Replacement functions To create the reduced model, we replaced f_A by $h_A = 0$.

Hyperparameters We selected the hyperparameters, α , β , and γ , from the following sets: $\alpha \in \{10^{-2}, 10^{-1}\}$, $\beta \in \{10^{-2}, 10^{-1}\}$, and $\gamma \in \{10^5, 10^6\}$. These ranges were chosen to roughly adjust the values of the corresponding regularizers to that of the ELBO. The configuration that achieved the best reconstruction error on the validation set was selected finally: $\alpha = 10^{-1}$, $\beta = 10^{-2}$, and $\gamma = 10^6$. In computing $R_{DA,2}$, we sampled z_P^* from the uniform distribution on range $[0.005, 0.2]$.

Optimization We used the Adam optimizer with its⁹ $\alpha = 10^{-3}$, $\gamma_1 = 0.9$, $\gamma_2 = 0.999$, and $\epsilon = 10^{-3}$. We ran iterations with mini-batch size 200 for 20000 epochs (i.e., 100,000 iterations in total) and saved the model that achieved the best validation reconstruction error.

E.4 Galaxy images

Data property We used images of galaxies from a part of the Galaxy10 dataset¹⁰. We selected the 589 images of the ‘‘Disk, Edge-on, No Bulge’’ class to form an overall dataset. Each image is of size 69×69 with three channels, so $\mathbf{x}_i \in \mathbb{R}^{69 \times 69 \times 3}$. We normalized the intensity values into range $[0, 1]$.

¹⁰The original images are from the Sloan Digital Sky Survey www.sdss.org, and the labels are from the Galaxy Zoo project www.galaxyzoo.org. The dataset is available a part of the `astroNN` package [49]

Train/valid/test split We separated the overall dataset them into training, validation, and test sets with 400, 100, and 89 images, respectively. In training, we performed data augmentation with random vertical/horizontal flips and random rotation, and thus the size of the training set was 8,000.

Physics model The physics model $f_P : \mathbb{R}^4 \rightarrow \mathbb{R}^{69 \times 69}$ is an exponential profile of the light distribution of galaxies whose input is $\mathbf{z}_P := [I_0 \ A \ B \ \vartheta]^\top \in \mathbb{R}_{>0}^4$, whose elements have the semantics introduced in the following. Let $[f_P]_{i,j}$ denote the (i, j) -element of the output of f_P . Then, for $1 \leq i, j \leq 69$,

$$[f_P]_{i,j} = I_0 \exp(-r_{i,j}),$$

where

$$\begin{aligned} r_{i,j}^2 &:= \frac{(X_j \cos \vartheta - Y_i \sin \vartheta)^2}{A^2} + \frac{(X_j \sin \vartheta + Y_i \cos \vartheta)^2}{B^2}, \\ X_j &:= 2 \cdot \frac{j-1}{68} - 1, \\ Y_i &:= -2 \cdot \frac{i-1}{68} + 1. \end{aligned}$$

(X_j, Y_i) is the coordinate on the 69×69 even grid on $[-1, 1] \times [-1, 1]$. I_0 determines the overall magnitude of the light distribution, A and B determine the size of the ellipse of the light distribution, and ϑ determines its rotation. This model was used in a similar problem of Aragon-Calvo and Carvajal [5], where they only handle artificial images. See also, e.g., Erwin [23], for an extensive list of such light distribution models of galaxies.

Latent variables $\mathbf{z}_P \in \mathbb{R}^4$ contains the information of intensity, semi-major and semi-minor axes, and rotation, as mentioned above. We used $\mathbf{z}_A \in \mathbb{R}^2$ in the full NN+phys and NN+phys+reg models. Meanwhile, we used $\mathbf{z}_A \in \mathbb{R}^6$ (and no \mathbf{z}_P) in the NN-only model.

Decoder architecture There is no nontrivial equation-solving process this time because the physics model f_P itself gives the closed-form solution. So the data-generating process in the full NN+phys and NN+phys+reg models is:

$$\mathcal{F}[f_P, f_{A,\text{Unet}}, f_{A,\text{tconv}}; \mathbf{z}_P, \mathbf{z}_A] := f_{A,\text{Unet}}(f_P(\mathbf{z}_P), f_{A,\text{tconv}}(\mathbf{z}_A)).$$

$f_{A,\text{tconv}}$ is a neural net with transposed convolutional layers and given \mathbf{z}_A , outputs a signal in $\mathbb{R}^{69 \times 69}$. $f_{A,\text{Unet}}$ is a neural net with architecture similar to the U-Net, whose outputs are in $\mathbb{R}^{69 \times 69 \times 3}$. We used the rectified linear unit (ReLU) as activation function and applied batch normalization before each activation function. In the NN-only model, we modeled $f_A(\mathbf{z}_A)$ only with a neural net with transposed convolutional layers whose output is in $\mathbb{R}^{69 \times 69 \times 3}$.

Note that we do not consider the NN+solver type of baseline as there appear no nontrivial solvers.

Encoder architecture The architecture of $g_{P,2}$ and g_A is similar to the one in Aragon-Calvo and Carvajal [5]. We put the softplus function after the final output of g_P to make its output positive-valued. $g_{P,1}$ is simply $g_{P,1}(\mathbf{x}) := \sum_{i=1}^3 c_i[\mathbf{x}]_i$, where $[\mathbf{x}]_i$ denotes the i -th channel of \mathbf{x} , and c 's are trainable parameters.

Replacement functions To create the reduced model, we replaced $f_{A,\text{Unet}}$ by h_A such that $h_A(\boldsymbol{\nu}) := [\boldsymbol{\nu}; \boldsymbol{\nu}; \boldsymbol{\nu}] \in \mathbb{R}^{69 \times 69 \times 3}$ (i.e., the repeat operator along the channel axis).

Hyperparameters We selected the hyperparameter α from $\alpha \in \{10^{-2}, 10^{-1}, 1\}$. This range was chosen to roughly adjust the value of the corresponding regularizer to that of the ELBO. The others were fixed to be $\beta = 1$ and $\gamma = 10^3$; these values were also determined by roughly adjusting the order of the values of objectives. In computing $R_{\text{DA},2}$, we sampled from the uniform distributions on $I_0^* \in [0.5, 1]$, $A^* \in [0.1, 1.0]$, $e^* \in [0.2, 0.8]$, and $\vartheta^* \in [0, 3.142]$, where $B = A(1 - e)$.

E.5 Human gait

Physics model We modeled f_P with a trainable Hamilton's equation as in [91, 29]:

$$f_P \left(\begin{bmatrix} \mathbf{p}^\top & \mathbf{q}^\top \end{bmatrix}^\top, \mathbf{z}_P \right) = \begin{bmatrix} -\frac{\partial \mathcal{H}}{\partial \mathbf{q}}^\top & \frac{\partial \mathcal{H}}{\partial \mathbf{p}}^\top \end{bmatrix}^\top,$$

where $\mathbf{p} \in \mathbb{R}^{d_H}$ is a generalized position, $\mathbf{q} \in \mathbb{R}^{d_H}$ is a generalized momentum, and $\mathcal{H}: \mathbb{R}^{d_H} \times \mathbb{R}^{d_H} \rightarrow \mathbb{R}$ is a Hamiltonian. We let $d_H = 3$ and modeled \mathcal{H} with an MLP with two hidden layers of size.

Latent variables $\mathbf{z}_P \in \mathbb{R}^{2d_H}$ is used as the initial condition of \mathbf{p} and \mathbf{q} . There was also $\mathbf{z}_A \in \mathbb{R}^{15}$.

Decoder architecture In the full NN+phys and NN+phys+reg models, the decoding process contains a numerical solver of ODE $f_P = 0$ with the Euler method. Its output is then transformed by f_A , an MLP with two hidden layers of size 512.

Encoder architecture g_P and g_A are MLPs with five hidden layers of size 512, 512, 512, 64, 32.

Replacement functions To create the reduced model, we replaced f_A by an affine map h_A , where h_A is applied to each snapshot of a sequence independently.

Hyperparameters We selected the hyperparameter α from $\alpha \in \{10^{-3}, 10^{-2}, 10^{-1}, 1\}$. This range was chosen to roughly adjust the value of the corresponding regularizer to that of the ELBO. The other hyperparameters were just $\gamma = \beta = 0$ as we did not use the corresponding regularizers.

F Additional experimental results

We present additional experimental results including investigation of the sensitivity of hyperparameter values and some observation on training runtime.

F.1 Forced damped pendulum

Hyperparameter sensitivity We investigated the sensitivity of the performance with regard to the hyperparameters, i.e., the regularization coefficients, α , β , and γ . We varied them around the nominal values, i.e., the setting with which the results were reported in the main text ($\alpha = 10^{-2}$, $\beta = 10^{-3}$, and $\gamma = 10^{-1}$; see also Appendix E). Figure 7 summarizes the result. We can consistently observe the tendency that 1) NN+phys+reg is far better than phys-only in terms of the reconstruction error (upper row); and that 2) NN+phys+reg is far better than NN+phys in terms of the estimation error of physics parameter ω (lower row).

Achieved hyperparameter values We examined the values of the regularizers for data augmentation. After training, $R_{DA,1} \approx 0.5$ and $R_{DA,2} \approx 2 \times 10^{-3}$ whereas $\|x\|_2^2 \approx 16$ on average. This result implies that the functionality of $g_{P,1}$ and $g_{P,2}$ are well controlled as intended.

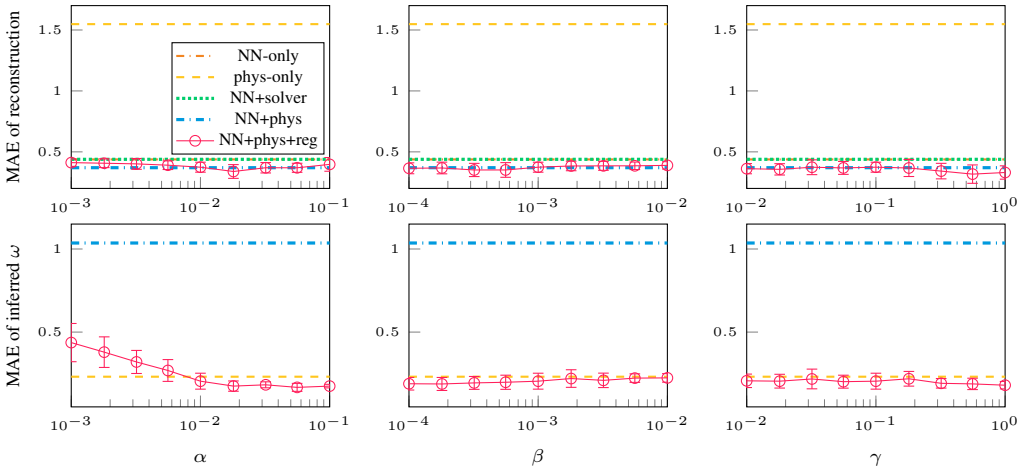


Figure 7: Performances on the pendulum data with one of the hyperparameters (α , β , or γ) varied around the nominal value, while the others maintained. Averages and SDs over five random trials are reported. Reference values are shown in dashed or dotted lines.

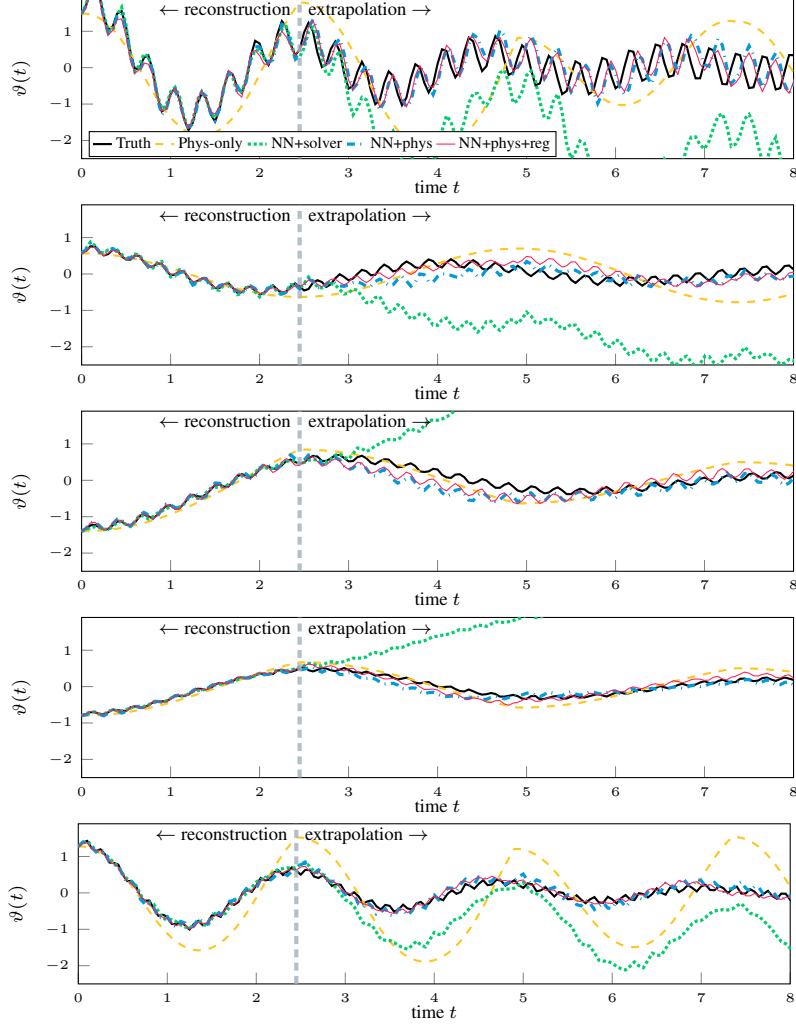


Figure 8: Reconstruction and extrapolation of five test samples of the pendulum data. Range $0 \leq t < 2.5$ is reconstruction, whereas $t \geq 2.5$ is extrapolation. The bottom corresponds to the example presented in the main text.

Training runtime In training, the NN-only model took about 5.13 seconds for 10 epochs, and the NN+phys+reg took about 10.9 seconds for 10 epochs, though we believe our implementation can still be improved for more efficiency. The difference probably stems from the physics-part encoder.

More examples of reconstruction and extrapolation In the main text, we have shown only one example case of the reconstruction and extrapolation. In Figure 8, we provide more examples on different test samples to facilitate further understanding of the result.

E.2 Advection-diffusion system

Hyperparameter sensitivity We investigated the sensitivity of the performance with regard to the hyperparameters α , β , and γ . We varied these values around the nominal values, i.e., the setting with which the results were reported in the main text ($\alpha = 10^{-1}$, $\beta = 10^{-2}$, and $\gamma = 10^6$; see also hyperparameter settings in Appendix E). Figure 9 summarizes the result. Across all the coefficient values, we can consistently observe the tendency similar to that in the pendulum data experiment.

Table 2: Performances on test set of the galaxy image data. Averages (and SDs) over the whole test set are reported.

	MAE of reconstruction	
NN-only	0.0167	(3.0×10^{-2})
Phys-only	0.0264	(3.9×10^{-2})
NN+phys(+reg), $\alpha = 0$	0.0188	(3.4×10^{-2})
NN+phys+reg, $\alpha > 0$	0.0180	(3.3×10^{-2})

Table 3: Performances on test set of the gait data. Averages (SDs) over 20 random trials are reported.

	MAE of reconstruction	
Phys-only	0.726	(1.0×10^{-2})
NN+solver	0.276	(1.5×10^{-2})
NN+phys	0.273	(9.0×10^{-3})
NN+phys+reg	0.259	(9.0×10^{-3})

Achieved hyperparameter values We examined the values of the regularizers for data augmentation. After training, $R_{DA,1} \approx 0.01$ and $R_{DA,2} \approx 5 \times 10^{-7}$ whereas $\|x\|_2^2 \approx 458$ on average. This result implies that the functionality of $g_{P,1}$ and $g_{P,2}$ are well controlled as intended.

Training runtime In training, the NN-only model took about 6.01 seconds for 10 epochs, and the NN+phys+reg took about 15.4 seconds for 10 epochs.

F.3 Galaxy images

Reconstruction In Figure 10, we show examples of reconstruction of five test samples. While the phys-only model cannot recover the color information by construction, the other models that include neural nets reproduce the original colors to some extent. The reconstruction errors over the whole test set are reported in Table 2. From these results, we can observe that the reconstruction performance is similar between NN-only, NN+phys, and NN+phys+reg. Despite the similar reconstruction performance, the NN+phys+reg model achieves clearly better generation performance as shown in the main text.

Counterfactual generation In Figure 11, we show the result of generation, where we varied the last element of z_P that corresponds to the angle of a galaxy in image, ϑ . We examined the models trained without or with one of the regularizers, R_{PPC} (i.e., $\alpha = 0$); the other regularizers were always active. In Figure 11, the case without the regularizer does not show reasonable generation with different ϑ . Note that $\vartheta < 0$ was never encountered during training as we set the range of the last element of z_P to be non-negative; nevertheless reasonable images are generated with $\vartheta < 0$.

Latent variable We computed the first two principal scores of z_A and plotted them with the corresponding image sample in Figure 12. In the NN-only model, the distribution of z_A clearly

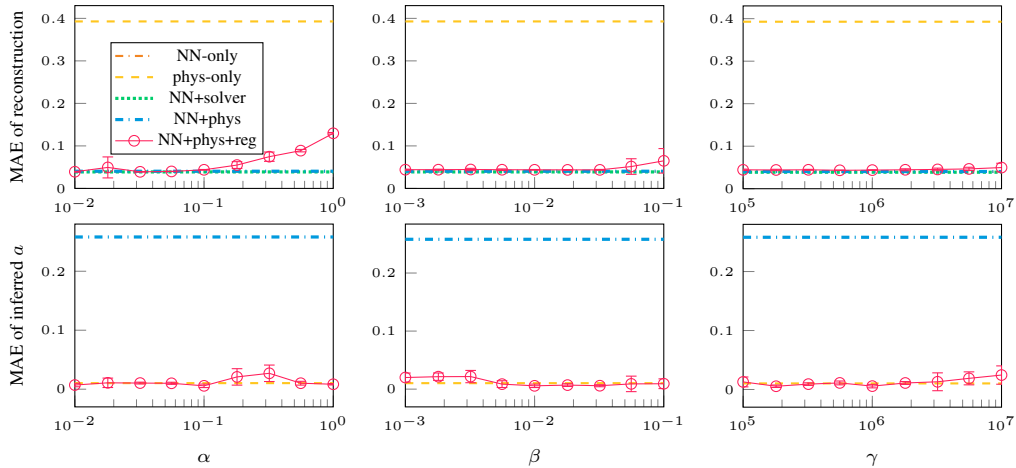


Figure 9: Performances on the advection-diffusion data with one of the hyperparameters (α , β , or γ) varied around the nominal value, while the others maintained. Averages and SDs over five random trials are reported. Reference values are shown in dashed or dotted lines.

corresponds to the angle of the galaxy in images¹¹. In contrast in the NN+phys+reg model, such a correspondence is not observed. This is a reasonable result because in NN+phys+reg, the semantic of galaxy angle is completely assigned to the last element of z_P .

F.4 Human gait

Reconstruction The reconstruction errors over the whole test set are reported in Table 3.

G Extension

While the proposed framework is useful as shown in our experiments, there are several directions to go for possible technical improvement of the method. First, physics-integrated VAEs can be further combined with techniques to solve ODEs and PDEs with neural networks [71, 101, 100]. We supposed the use of differentiable numerical solvers if the model contains ODEs or PDEs, but such numerical solvers are often computationally heavy. Replacing them with neural net-based solutions will be useful for various applications. Second, while we defined the regularizer based on the (possibly loose) upper bound of KL divergence, we may use other dissimilarity measure of distributions or random variables, such as maximum mean discrepancy. Third, the proposed regularization method can be extended to other types of deep generative models; e.g., an extension to InfoVAE [111] is straightforward. Lastly, neural architecture search in the context of physics-integrated models [7] would be an interesting topic also in generative modeling.

¹¹This might be a good property in some applications, but we do not want for it to happen in our NN+phys+reg model because the angle is rather manually encoded in an element of z_P , and z_A should carry other information.

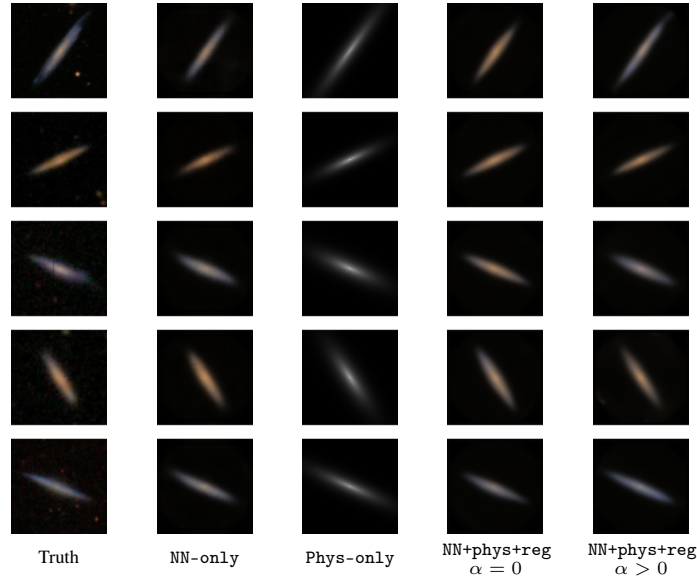


Figure 10: Reconstruction of five test samples of the galaxy images data. Best viewed in color.

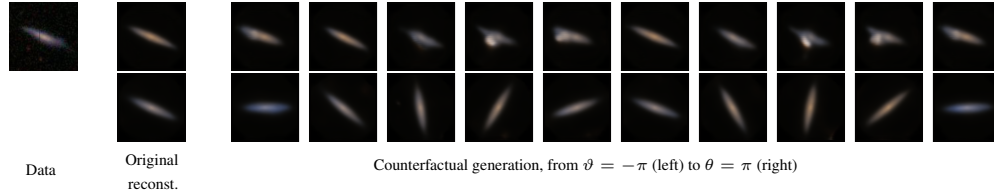


Figure 11: Counterfactual generation for the galaxy image data. (1st column) Original data sample. (2nd column) Original reconstruction of the sample. (the rest) Generation with varying $[z_P]_4$, which corresponds to the angle of galaxy in an image, ϑ , from $-\pi$ to π . The upper row is with NN+phys(+reg) with $\alpha = 0$, and the lower row is with NN+phys+reg with $\alpha > 0$.

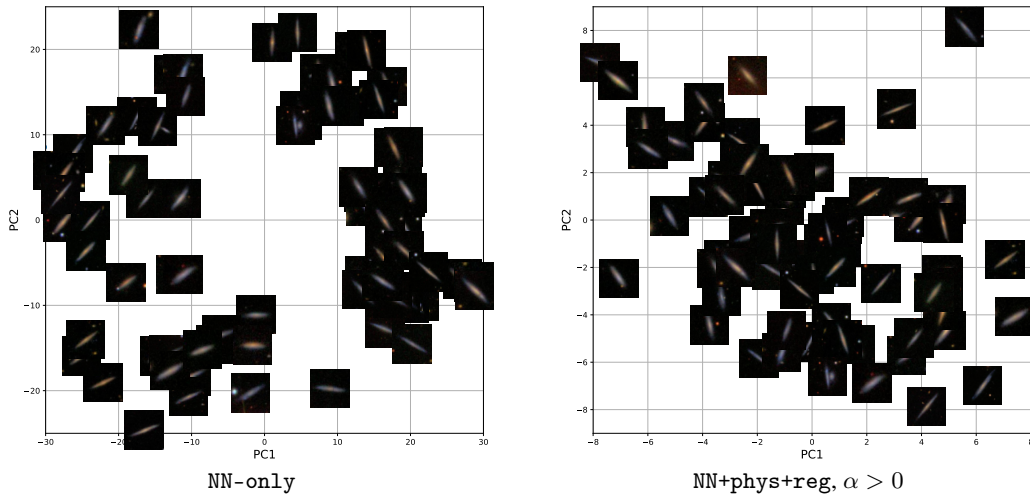


Figure 12: Visualization of latent variable z_A learned from the galaxy image data. The corresponding test data samples are shown at the points specified by the first two principal scores of z_A .